Supplemental Information

Noncooperative Interactions between Transcription
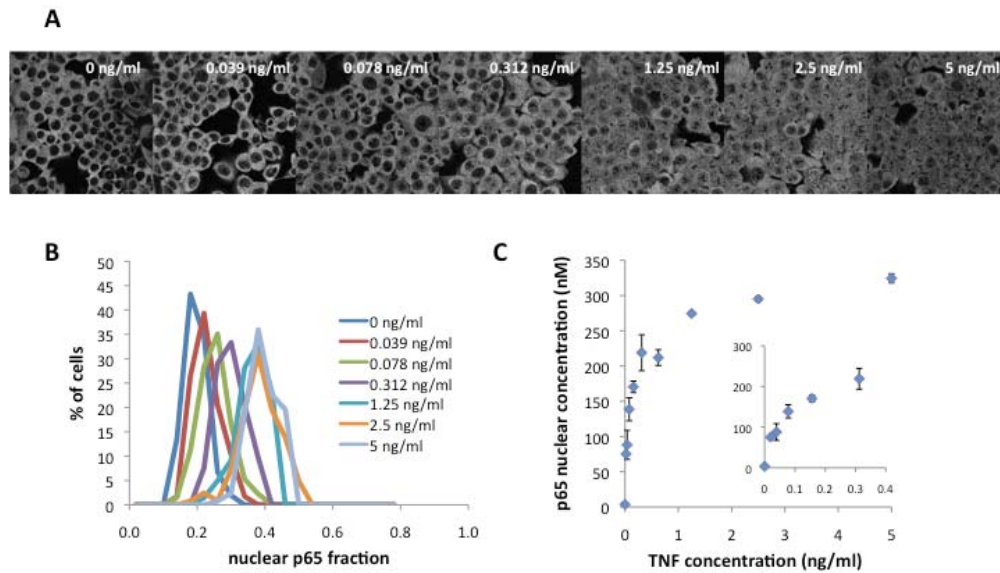
Factors and Clustered DNA-Binding Sites Enable

Graded Transcriptional Responses to Environmental Inputs

**Luca Giorgetti, Trevor Siggers, Guido Tiana, Greta Caprara,
Samuele Notarbartolo, Teresa Corona, Manolis Pasparakis,
Paolo Milani, Martha L. Bulyk, and Gioacchino Natoli**

Figure S1 (related to Figure 2). Increasing doses of TNFα determine a gradual increase in NF-kB p65 nuclear concentration.

(A) Wild-type HCT 116 cells were stimulated with increasing doses of TNFα for 20 minutes. The nuclear translocation of NF-kB was assessed by immunofluorescence with an anti-p65 antibody. Confocal sections of cell populations treated with different doses of TNFα are shown.

(B) Quantitative analysis of immunofluorescence. We acquired confocal sections of each of the samples shown in panel A (>5 independent fields per sample, corresponding to *n>150* cells per sample). We identified cell nuclei by applying an intensity threshold on the DAPI channel. After constructing binary masks corresponding to nuclear and cytoplasmic compartments, we quantified the p65 signal in each compartment and calculated the nuclear fraction of the signal on a cell-by-cell basis. We then plotted the distribution of nuclear-over-total p65 signal for all the samples considered. The distributions are unimodal and their median value shifts uniformly to higher nuclear values when increasing the TNFα dose, showing that increasing TNFα doses induce uniformly increasing nuclear localization of NF-kB in the cell population.

(C) We used a quantitative ELISA assay coupled to confocal measurements of the average nuclear volume of HCT 116 cells (see Materials and Methods in the manuscript) to measure the average nuclear concentration of p65 as a function of the TNFα dose (after 20 minutes stimulation). The inset provides a magnification of the low-TNFα regime.
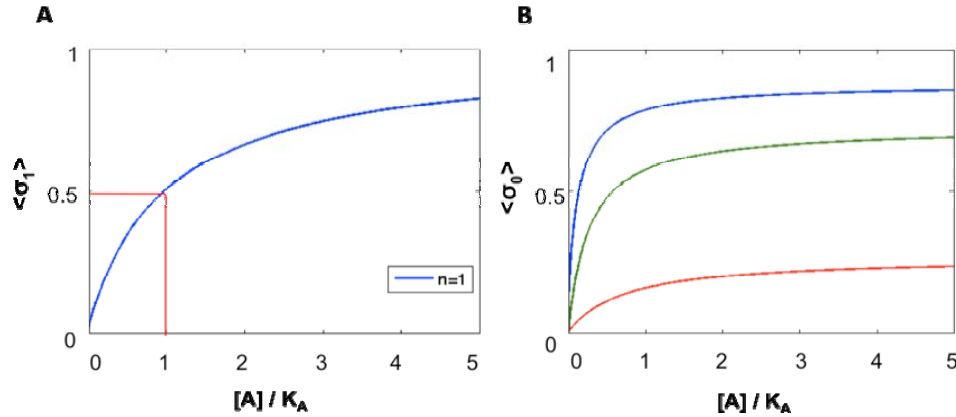
Figure S2 (related to Figure 3). Model predictions in the case where only one NF-kB binding site is present (n=1).

(A) Mean NF-kB binding site occupancy as a function of NF-kB nuclear concentration.

(B) Mean Pol II occupancy on the core promoter as a function of NF-kB nuclear concentration. Blue: $J=2k_BT$, $L=-4k_BT$; Red: $J=5k_BT$, $L=-4k_BT$; Green: $J=5k_BT$, $L=-6k_BT$. Concentrations were renormalized to the NF-kB binding constant.

Discussion to Figure S2

We show here that the presence of more than one NF-kB binding site is necessary to ensure that the induction profiles of *NFKBIA* can be fitted by the different model variants. Specifically, we show that a model with only one binding site would not predict correctly the convexity of the observed *NFKBIA* induction profile.

First, we notice that the three models are identical for n=1 (where n stands for the number of NF-kB binding sites). The differences among the three models arise when n>1, as models differ by the different logics of interaction between bound NF-kB and the Pol II complex when more than one site is occupied. Thus, the considerations that follow may be referred to any of the three models.

When only one NF-kB binding site is located in the promoter (say site 1, while site 0 represents the core promoter where Pol II exchanges), its occupancy is given by

$$\langle \sigma_1 \rangle = \frac{1}{1 + \dfrac{K_A}{[A]}},$$

where K_A is the NF-kB binding constant and [A] the NF-kB nuclear concentration. The behavior of $\langle \sigma_1 \rangle$ as a function of [A] is therefore hyperbolical (see Supplementary Figure 2A), reaching half saturation when $[A]=K_A$, as expected in the case of a simple binding process.

The Pol II occupancy of the core promoter, $\langle \sigma_0 \rangle$, is affected by the interaction with this binding site only, and its expression is given by

3

$$\langle \sigma_0 \rangle = \cfrac{1}{1 + \cfrac{1}{F(A)} \cfrac{K_P}{[P]}},$$

where [P] is the concentration of free polymerases, K_P the Pol II binding constant to the core promoter, and F(A) a function that contains all the contributions from NF-kB binding and NF-kB/Pol II interactions (see Eq. (22) in the Supplementary Description of the thermodynamic model):

$$F(A) = \cfrac{1 + \cfrac{[A]}{K_A} e^{-\frac{L}{k_B T}}}{1 + \cfrac{[A]}{K_A}}$$

Thus, the absolute value of $\langle \sigma_0 \rangle$ depends on the values of two parameters: L, setting the NF-kB/Pol II interaction strength; and J=-k_BT log(P/K_P), setting the basal transcription level. However, the behavior of $\langle \sigma_0 \rangle$ as a function of the NF-kB concentration remains hyperbolical (Supplementary Figure S2B). By contrast, the *NFKBIA* induction profile has a slightly sigmoidal profile (see Figure 4A in the main text). Therefore, irrespective of the choice of parameter values, a model with one site won't be able to fit the experimental data accurately.
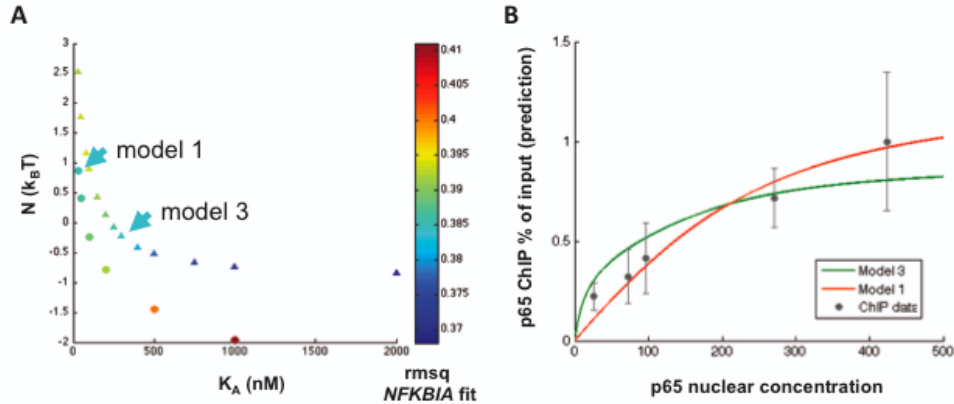
Figure S3 (related to Figure 4). Equivalent model parameterizations return experimentally distinguishable predictions.

(A) The root-mean-square values of the fits to the *NFKBIA* profile obtained with Model 1 (circles) and Model 3 (triangles) are plotted as a function of the imposed value of the NF-kB binding constant K_A and the best estimate of the free parameter N (controlling the strength of NF-kB binding cooperativity). The fit was performed with 6 kB sites in the *NFKBIA* promoter. Markers are colored according to the rmsq value (red: bad fit; blue: good fit). See Tables 1 and 3 in the supplementary Analysis and fitting of transcriptional induction profiles to compare the rmsq, N and K_A values. Arrowheads mark two parameter sets that return a fit with rmsq≈0.385.

(B) The two parameter sets marked in panel A were used to predict the p65 occupancy profile on the cluster of 6 sites in the promoter. The two predictions show remarkably different rmsq values from the ChIP data, shown as gray markers (rmsq=0.0021 for Model1, 0.0012 for Model 3).

Discussion to Figure S3

The three models can be parameterized to fit each other, as it can be clearly seen in Figures 1, 4 and 6 of the supplementary "Analysis and fitting of transcriptional induction profiles", where all the three variants fit the *NFKBIA* induction profile with similar root-mean-square (rmsq) values. However, the regions of parameter space that return fits with similar quality are clearly separated, as exemplified in Supplementary Figure S3A for Models 1 and Model 3 (the two best-performing variants), where we plotted the rmsq value as a function of the imposed binding constant K_A and the best estimate of parameter N (setting the strength of binding cooperativity) obtained in the fit. Parameter sets that return fits with similar rmsq distances to the data (as the two indicated by arrowheads in Supplementary Figure 3A, both with rmsq≈0.385) have significantly different values of the NF-kB binding constant K_A (30 nM in the case of Model 1 vs. 300 nM in the case of Model 3) and the strength of binding cooperativity (N=0.8 k_BT for Model 1 vs. N=-0.2 k_BT for Model 3). These two parameter sets are sufficiently separated for the two models to produce qualitatively and quantitatively different predictions for the profile of NF-kB recruitment to the cluster, which we directly challenged in an independent experiment (see Figures 2, 5, and 8 in the supplementary "Analysis and fitting of transcriptional induction profiles" and Fig. 4b in the manuscript). In the case of the two parameter sets considered in Supplementary Figure S3, the root mean square distances of model predictions against the ChIP experiment were significantly different, and supporting Model 3 with a rmsq=0.0012 vs. 0.0021 for Model 1.

Thus, the different models can indeed be parameterized to fit each other, as it can be expected from having 4 free parameters and predicting a monotonous function. Nevertheless, we provide an independent way of distinguishing between promoter configurations represented by these parameter sets by predicting an independent observable, which we experimentally measured (Figure 4B in the main text and Supplementary Figure S3B). This is a crucial point in our analysis, which does NOT rely entirely on fitting procedures – rather on a combination of fitting and challenging predictions against new experimental data.
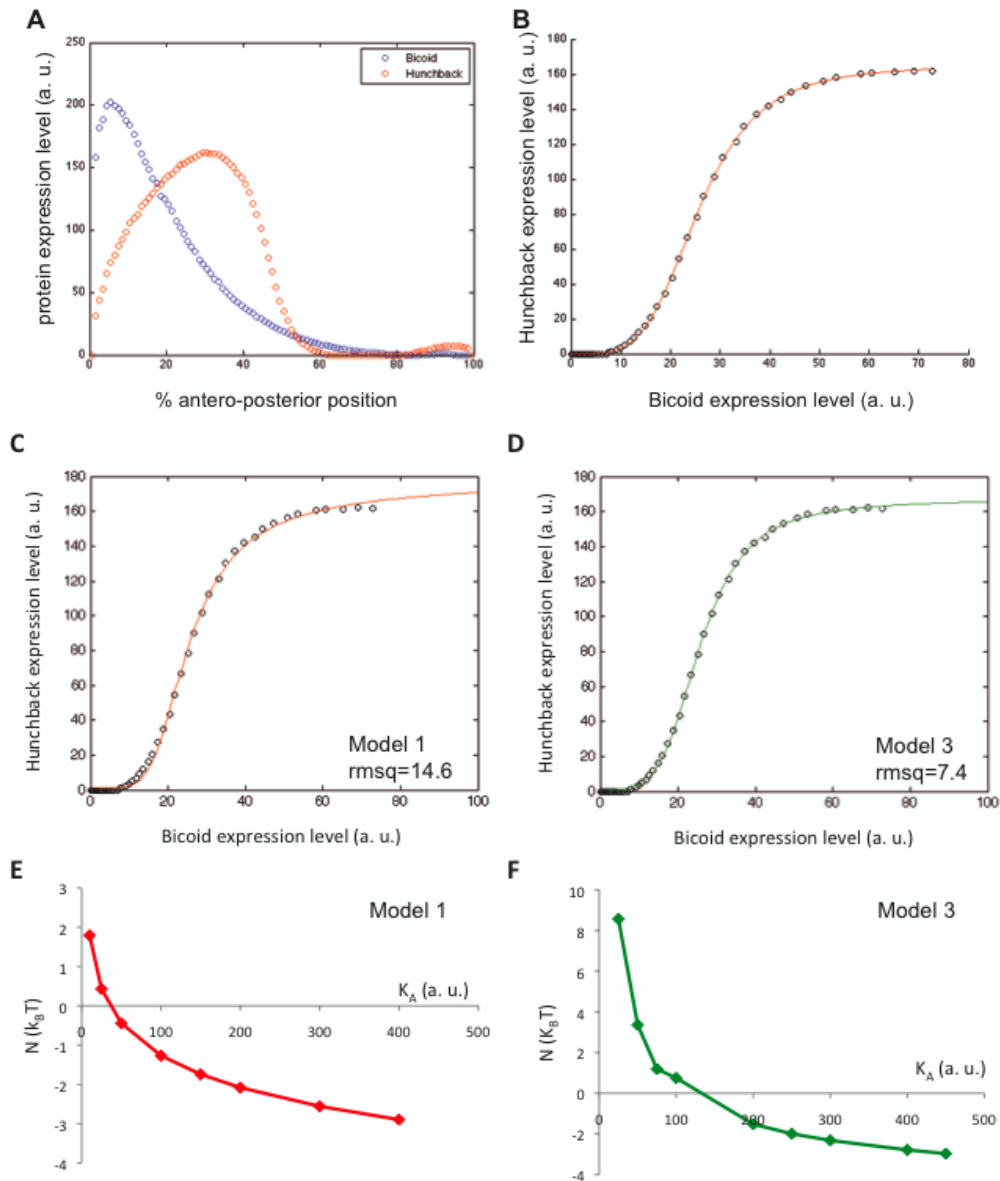
Figure S4. Model fits to the Bicoid/Hunchback induction profile in *Drosophila*.

(A) Bicoid (Bcd) and Hunchback (Hb) signals (integrated across the dorso-ventral direction over the 10% stripe along the embryo midline, retrieved from the FlyEx database, http://flyex.ams.sunysb.edu/flyex/). Quantitative fluorescence data (in arbitrary units) were plotted as a function of the antero-posterior position of a single wild-type *D. melanogaster* embryo at developmental stage 14A.

(B) Hunchback vs. Bicoid expression levels around the antero-posterior midline. Experimental points were fitted with a Hill curve, returning a Hill coefficient of 4.16 (red line).

(C-D) Model 1 and Model 3 fits to the Bicoid/Hunchback expression induction profiles for K_A=200 (in arbitrary immunofluorescence units) and in the presence of 7 Bicoid binding sites in the Hunchback promoter. Root-mean-square values are in fluorescence units.

(E-F) The values of parameter N (N>0: Bicoid binding anti-cooperativity; N<0: binding cooperativity) extracted from the fits at the different fixed values of K_A

Discussion to Figure S4

We chose to consider the Bicoid/Hunchback system in *D. melanogaster* as a model where TF binding cooperativity has been unequivocally demonstrated in vitro. We retrieved quantitative data of the Hunchback and Bicoid expression levels from the FlyEx database (http://flyex.ams.sunysb.edu/flyex/). We used data obtained in a single wild-type (Oregon R) embryo at stage 14A and integrated over the dorso-ventral direction across the central 10% stripe along the embryo midline (Supplementary Figure 4A). In this dataset, protein expression levels are expressed in arbitrary units, reflecting the fluorescence intensity from the stained proteins in the nuclei of a fixed embryo (*not* actual concentration values) after background subtraction. We extracted the data from the central part of the embryo around the antero-posterior midline (namely the region where Bicoid induces the expression of Hunchback), and plotted the Hunchback vs. Bicoid expression levels in this region (Supplementary Figure 4B). The resulting input/output function could be fitted with a Hill equation with a Hill coefficient of 4.16, indicating a strongly cooperative Hunchback induction.

The Hunchback promoter has been reported to contain 7 Bicoid binding sites (Ma et al., Development 122, 1195-1206, 1996) whose in vitro binding affinity has been estimated to be in the range $K_A = 0.3 \div 460$ nM (see Ma et al. and Burz et al., EMBO J 17, 5998–6009, 1998), possibly reflecting different experimental conditions and *in vitro* assays. Thus, as in the case of NF-kB, the Bicoid binding affinity is subject to a huge uncertainty, with in vitro measurements spanning four orders of magnitude. As the FlyEx data are reported in arbitrary fluorescence units (being based on non-calibrated fluorescence measurements) we had to convert these affinity data into values that could be compared with the Bicoid expression levels. By using the quantitative measurements of Bicoid concentrations in Gregor et al., where the maximal concentration of Bicoid in an early stage 14 embryo was found to be approximately 55 nM, we could convert the range of K_A concentrations into fluorescence units and obtain that the expected values of *in vitro* measured K_A's lie in the range $0.5 \div 500$ fluorescence units.

We chose to adopt the same strategy that we used to fit the *NFKBIA* induction profile, and imposed different values of binding affinities K_A before fitting the Hunchback profile with the other four parameters. We fitted the data with all the three variants of the model (Model 1: All-or-none recruitment of Pol II by bound TFs; Model 2: non-additive recruitment of Pol II; Model 3: additive Pol II recruitment).

We did not find acceptable fits using Model 2. Even in the presence of strong Bicoid binding cooperativity, the non-additive design of TF/Pol II interactions can never describe the strong sigmoidality of the Bicoid/Hunchback response curve (data not shown). Notice that also when fitting the *NFKBIA* profile, Model 2 was the worst performing variant.

By contrast, Models 1 and 3 could fit the Hunchback induction profile in the whole range of *in vitro* measured K_A (Supplementary Figure S4C-D). Both models returned a significant amount of Bicoid binding cooperativity ($N < -0.5$ k_BT) in a wide range of *in vitro* binding constants (Supplementary Figure S4E-F). Thus, our model detects binding cooperativity in a system that is known to operate in a strongly cooperative manner. Model 3 (additive Pol II recruitment) was more accurate in fitting the induction profile (with rmsq values roughly half of those returned by Model 1, see Supplementary Figure S4C-D and data not shown for the other imposed K_A values).

We also adopted the following alternative approach to data fitting. Given that Bicoid binding cooperativity has been demonstrated *in vitro*, we imposed fixed arbitrary strengths of binding cooperativity, corresponding to fixed values of the parameter N ($N < 0$), and used K_A as a free parameter in the fit. Again, for each value of N we found a K_A value in the range of the in vitro measured binding constants (data not shown). This shows again that our model detects and coherently describes also a cooperative system.
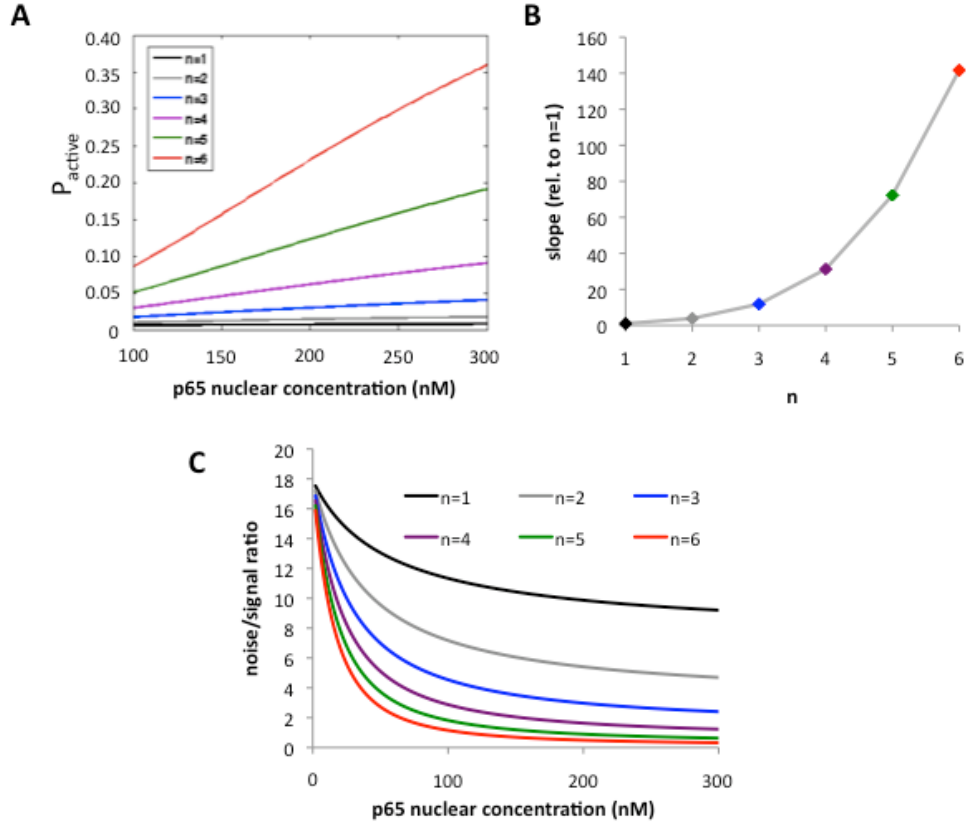
Figure S5. The number of NF-kB binding sites impacts on the dynamic range of transcription and the intrinsic transcriptional noise.

(A) The number of kB sites determines the sensitivity of the transcriptional response to changes in NF-kB concentration. We calculated the transcriptional activation of genes with 1 to 6 kB promoter-proximal NF-kB binding sites under the experimentally determined conditions of additive Pol II recruitment in the absence of NF-kB binding cooperativity (K_A=200 nM), as a function of p65 nuclear concentration. The plot shows a magnification of the linear part of the curves, in the 100-300 nM range. The sensitivity to changes in TF concentration (i.e. the slope of the curve) increases when increasing the number of kB sites.

(B) The slope of the curves shown in panel A was renormalized to the slope of the n=1 case, then potted against the number of kB sites. Increasing the number of sites from 1 to 6 leads to a dramatic increase in the sensitivity to changes in NF-kB concentration.

(C) The intrinsic component of transcriptional noise, identified as the magnitude of equilibrium fluctuations in Pol II occupancy of the core promoter at a given p65 concentration (please refer to the description of the model in the Supplementary Information), is dependent on the number of NF-kB binding sites. We plotted the noise over signal ratio (i.e. the ratio of the mean square deviation of Pol II occupancy, $\delta\sigma_0$, over the average Pol II occupancy $<\sigma_0>$) versus the p65 nuclear concentration, for genes with 1 to 6 NF-kB binding sites. As in panel A, we ran the model in the identified regime of additive Pol II recruitment in the absence of NF-kB binding cooperativity.

8
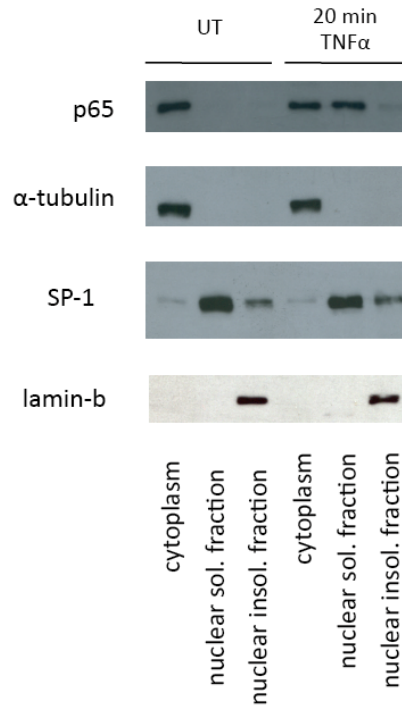
Figure S6. Most nuclear p65 is retained in the nuclear extracts that were used for ELISA quantification. p65 was detected in western blot in the cytoplasmic, nuclear soluble and insoluble fractions (identified by the presence α-tubulin, SP-1 and lamin-β, respectively) obtained from the same number of untreated and TNF-treated HCT 116 cells. Band quantification showed that >90% of nuclear p65 was extracted in the soluble nuclear fraction.
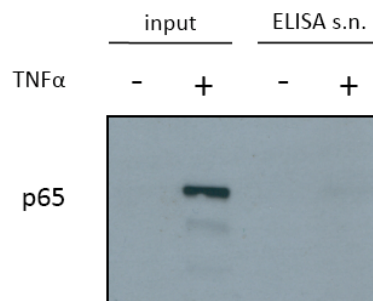
Figure S7. p65 was detected in western blot in soluble nuclear extracts before (input) and after (ELISA supernatant, s.n.) 1h incubation in an oligo-based ELISA well. The extract was entirely depleted of p65 during incubation, ensuring accurate p65 quantification.
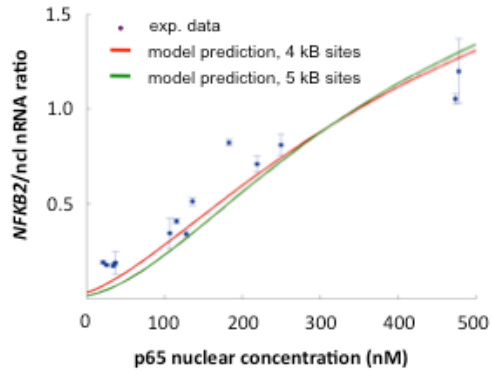
Figure S8. The experimental data and the predictions of Model 3 (in the identified regime of non-cooperative NF-kB binding and K_A=200 nM) concerning the transcriptional induction profile of *NFKB2*. The calculation was performed with 4 (red line) and 5 (green line) kB sites in the promoter.

SUPPLEMENTAL TABLE

	Forward primer	Backward primer
nRNA primers		
NFKBIA	TGAGGGTTGAAACAGGTGGT	GAAGCACCAACCTGAGCATT
NFKB1	TCTCCCCCATGTTAGAGTGC	AGTCAGCATCGCATCATCTG
NFKB2	CCTAGCCCAGAGACATGGAG	TCCTTTTGGAGGCAGAGTTG
IRF1	ACATCCCAGTGGAAGTTGTG	GTGCCAGGTGGAGTTCTGAT
TNFAIP3	TGGGACTCCAGAAAACAAGG	GAAAAGCACGGTAGGTCCTG
CSF1	GCAGGAGTATCACCGAGGAG	CCTATTTTCCTGCCTGCAAC
Nucleolin (NCL)	TAGGGCAGGTTTTCTGTTGG	CTCGACATTTCAGGCCATTC
ChIP primers		
NFKBIA promoter	GAAGGACTTTCCAGCCACTC	GGAATTTCCAAGCCAGTCAG

Table S1. Primers used in nRNA quantification and ChIP experiments.

SUPPLEMENTAL EXPERIMENTAL PROCEDURES

Analysis of nascent transcripts. All steps were performed on ice or at 4 °C. 6x106 cells were washed 3x in ice-cold PBS, and cytoplasmic membranes were lysed in 300 µl of lysis buffer (50 mM Tris pH 8.0, 2 mM EDTA pH 8.0, 0.1% NP-40, 10% Glycerol, 0.15 mM spermine, 0.5 mM spermidine, 1 mM DTT, 1 mM PMSF). Nuclei were pelleted through a 3-ml cushion of HB 0.9 M sucrose (10% glycerol, 0.9 M sucrose, 60 mM KCl, 15 mM NaCl, 1.5 mM HEPES, pH 7.9, 0.5 mM EDTA, 0.15 mM spermine, 0.5 mM spermidine, 0.5 mM PMSF, 1 mM DTT) by a 15-min centrifugation in microfuge at 3,750 rpm and resupended in 100 µl of nuclear suspension buffer (75 mM NaCl, 20 mM Tris-HCl, pH 7.5, 0.5 mM EDTA, 0.125 mM PMSF, 0.85 mM DTT, 50% glycerol, 100 g/ml yeast RNA). Nuclei were lysed on ice for 10 min in 7.5 volumes of a buffer containing 0.3 M NaCl, 20 mM HEPES, pH 7.6, 0.2 mM EDTA, 7.5 mM MgCl2, 1 M urea, 1 mM DTT, 1 % NP-40 and 100 g/ml yeast RNA. Chromatin was pelleted by 10 min at 13,000 rpm in a microfuge, and resuspended in 1 ml Trizol reagent (Invitrogen). Chromatin-associated transcripts were extracted following manufacturer's instructions, precipitated 2x in 2-propanol and ethanol and resuspended in 20 µl of dd-H2O. 1 µg of nascent transcripts were reverse-transcribed in a 10 µl volume using 25 pmol of random hexamers and M-MuLV Reverse Transcriptase RNase H (Finnzymes), then diluted in dd-H2O to a final volume of 100 µl. 4 µl of the diluted cDNA was quantified by RT-PCR with primers specific for pre-mRNA (designed to amplify either intronic regions, or regions lying across splicing junctions). Contamination from genomic DNA was excluded by running RT-PCR reactions with non-reverse transcribed samples.

ANALYSIS AND FITTING OF TRANSCRIPTIONAL INDUCTION PROFILES

Q-PCR quantification.

For all genes considered in the manuscript, we calculated the gene vs. nucleolin (*ncl*) nascent RNA (nRNA) ratio as $G=2^{-\Delta Ct}$, where $\Delta Ct = Ct_{gene}-Ct_{ncl}$ is the difference between the number of Q-PCR thermal cycles at threshold. Ct's were always averaged over two duplicate reactions (with associated errors σ_{gene} and σ_{ncl}). Nucleolin was chosen as a housekeeping gene as it provides robust data and it is constant throughout the stimulation.

Error bars on G (*y* axis in transcriptional induction profiles) represent errors in Q-PCR quantification of the gene/*ncl* ratio, which were obtained by propagating the errors on *Ct* duplicates:

$$\sigma_G = \ln(2) \cdot G \cdot \sqrt{\sigma_{gene}^2 + \sigma_{ncl}^2} \,.$$

Quantification of nuclear p65 concentration.

We employed TransAM NF-kB p65 colorimetric ELISA kits from Active Motif. In these kits, NF-kB dimers are captured by immobilized oligonucleotides containing consensus NFkB binding sites (5'-GGGACTTTCC-3'). This results in a quantification of the amount of functional NF-kB, i.e. the fraction of DNA binding-competent nucleoplasmic NF-kB (in this system consisting mainly of p65/p50).

To quantify the number of p65 molecules per nucleus, we loaded in duplicate a fixed amount of nuclear extract of each sample, corresponding to a known number of nuclei. Typically we loaded 3 μl out of the 50 μl total lysate, corresponding to 3/50th of the total number of nuclei in the original sample. We then processed the plate according to the manufacturer's instructions, and quantified the absolute quantity of functional p65 in each sample by using the provided recombinant p65 as a calibration standard. We also analyzed the post-reaction supernatant for residual NF-kB levels and verified a complete depletion (Supplementary Figure S4).

We found that the typical mean number of p65 molecules per nucleus spanned from ≈1,000 in unstimulated cells to ≈100,000 in cells stimulated for 20 minutes with TNFα.

To obtain the nuclear concentration of p65, we measured the mean nuclear volume of HCT116 cells. We stained with DAPI the nuclei of cells fixed in 4% paraformaldehyde and permeabilized with Triton 0.2%, then acquired confocal stacks of populations of nuclei. We used the Object Counter 3D ImageJ plug-in to reconstruct the three-dimensional shapes of the nuclei and measure their volume. We obtained an average nuclear volume of 720 ± 15 μm^3 (s.e.m., n=75). Accordingly, the mean p65 nuclear concentrations varied from 5 nM in unstimulated cells to ≈400 nM in cells stimulated with TNFα for 30 minutes. We considered the whole nuclear volume accessible to nucleoplasmic p65, in line with the recent observation that GFP-streptavidin diffuses also through nucleoli and heterochromatic domains [1].

Error bars on p65 concentrations represent the errors obtained from duplicate wells in ELISA assays, appropriately propagated during the calculation of concentrations.

Data fitting.

In order to fit the induction profile of *NFKBIA* with the thermodynamic model of promoter operation, we first merged the data obtained in experiments with increasing doses of TNFα and with p65 knock-down clones, given the excellent agreement of the datasets (see Fig. 2E in the manuscript).

The model contains six parameters:
1. n, the number of NF-kB binding sites ('kB sites') in the promoter;
2. J, the Pol II/promoter binding free energy;
3. K, the average NF-kB binding free energy to kB sites;
4. L, the NF-kB/Pol II interaction free energy;
5. N, the free energy associated to NF-kB binding to adjacent sites in the promoter;

6. α, the multiplicative constant rescaling Pol II binding probabilities to transcriptional activities in the units of the experimental output (gene/*ncl* nRNA ratio).

As a first step in the fitting procedure, we reduced the dimensionality of the parameter space in order to improve the robustness and reliability of parameter estimation. We kept 2 out of the 6 original model parameters fixed, proceeding as follows.

First, we fixed the number of sites in the *NFKBIA* promoter-proximal cluster to 6 (or 5, when considering only the conserved kB sites, see below), according to the results of our computational analysis (Table 1 in the manuscript).

Second, we wrote the parameter K as follows (see the detailed description of the model):

$$K = -k_B T \ln(\frac{[A]}{K_A})$$

where [A] is the nuclear concentration of NF-kB and K_A its binding constant to specific sites in the promoter. [A] enters the fit as the independent variable (*x* axis). Thus the 'real' parameter contained in K is K_A. We exploited recent in vitro data showing that K_A ranges from 20 to 300 nM [2, 3]. We assigned to K_A different values in the range above, then performed independent fits with the remaining parameters that could not be measured experimentally (namely the interaction energies *N, L* and *J*, describing the degree of NF-kB binding cooperativity, the NF-kB Pol II interaction, and the basal level of Pol II occupancy respectively), plus the multiplicative parameter α.

Our fitting routine, written in the Mathematica environment (Wolfram Research, Inc., Mathematica, Version 6.0, Champaign, IL (2007)), employed a Levenberg–Marquardt algorithm to implement the minimization of least squares [4].

As described below, we obtained acceptable fits of the *NFKBIA* induction profiles with all the three models, obtaining values for the free parameters that were dependent on the model and on K_A. Remarkably, for all models the estimates of the free parameters were acceptable (i.e. in the range of macromolecular interactions, on the order of few units of $k_B T$) for most of the attempted values of K_A. Nevertheless, one of the three models (Model 3, see below) could optimally recapitulate additional experimental observations regarding NF-kB recruitment to the *NFKBIA* cluster and the transcriptional induction of other NF-kB target genes.

Hereafter we give a detailed description of the fitting results with all the three model variants.


All kB sites (conserved + non-conserved).

We began by analyzing the data within the assumption that all (both conserved and non-conserved) kB sites identified in the promoter-proximal regions contribute to the regulation of NF-kB target genes. Upon this assumption, the *NFKBIA* transcriptional induction profiles are fitted with *n=6*. The number of kB sites of the other target genes are listed in Table 1 in the manuscript.

Model 1. All-or-none NF-kB-Pol II interaction.

First, we considered Model variant 1 (see the Supplementary information of our thermodynamic model of NF-kB dependent promoter operation), which requires that *every* binding site in the cluster must be bound before Pol II can interact with the *cis*-regulatory sequence.

The *NFKBIA* induction profile could be fitted in the whole range of *in vitro* measured K_A, and also for higher values of the binding constant (Fig. 1). The goodness of fit, measured via the root mean square distance to the experimental points, increased for low values of the binding constant, i.e. higher binding affinities (Fig. 1B). In this regime (low values of K_A), the fit returned "repulsive" interactions between cognate NF-kB binding sites (N>0, corresponding to a regime of binding anti-cooperativity) (see the detailed list of parameters in Table 1). Conversely, for low NF-kB binding affinities, NF-kB binding cooperativity was necessary to reproduce the slight sigmoidality of the curve at low p65 concentration, and to "drive" NF-kB recruitment to the promoter despite the low affinity.
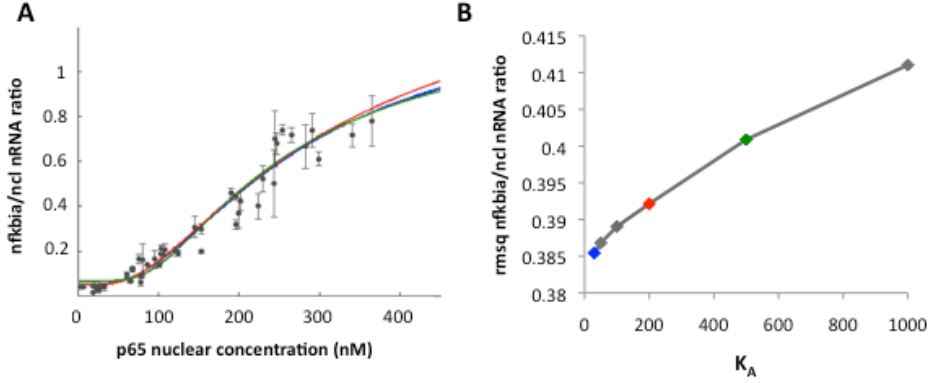
Figure 1. (A) Best fit of the *NFKBIA* induction profile with Model 1 obtained by imposing three values of the NF-kB binding constant. K_A was set to 30 nM (bue line), 200 nM (red line) and 500 nM (green line). The correlation coefficients associated with these fits are r=0.973, r=0.972 and r=0.970, respectively. (B) Root mean squares of the various fits obtained by imposing different values of K_A.

K_A (nM)	N	J	L	α	r (corr. coeff.)
30	0.86337	3.42668	-4.60444	1.55049	0.973185
50	0.413839	3.63656	-4.4327	1.9042	0.972991
100	-0.236622	4.55057	-4.18423	4.65884	0.972674
200	-0.78349	6.73652	-4.2104	44.8043	0.972231
500	-1.44074	7.06453	-4.4647	75.4677	0.97096
1000	-1.96901	6.839	-4.7052	69.096	0.969447

Table 1. Best estimates of the free parameters obtained by fitting the *NFKBIA* induction profiles with Model 1 for the various values of the NF-kB binding constants. Interaction parameters are expressed in units of k_BT. α and r stand for the multiplicative constant and the correlation coefficient, respectively.

Thus this variant of the model is able to reproduce the correct logic of operation of *NFKBIA* in a wide range of NF-kB binding constants, although the parameter sets obtained by imposing different values of K_A are diverse and suggest different interpretations concerning cooperativity in binding to kB sites. To challenge this interpretation of our experimental observations, we devised an independent experiment and measured the *in vivo* average binding occupancy of p65 onto the cluster of kB sites in the promoter of *NFKBIA*, as a function of nuclear p65 concentration. We stimulated a panel of HCT116 p65 knockdown clonal cell lines, each expressing a different residual level of p65, with 10 ng/ml TNFα for 20 minutes. We then performed chromatin immunoprecipitation (ChIP) with an antibody directed against p65, and quantified by Q-PCR the average p65 occupancy on the cluster of binding sites with primers specific for the *NFKBIA* promoter. We then plotted the p65 occupancy (normalized to the WT occupancy) vs. the p65 nuclear concentration (Fig. 2A, gray markers).

We used the parameter sets found in the *NFKBIA* fit and asked the model to predict the average recruitment of p65 on the promoter cluster (corresponding to the quantitiy $<\sigma_i>$, see the description of the model for the details) for a gene with 6 kB sites. We repeated the calculation for each of the parameter sets, and we rescaled each predicted profile of kB site occupancy with an adequate multiplicative factor to compare it to the ChIP data (whose value was determined by minimizing the root mean squares of the model prediction vs. the experimental data). Among all parameter sets, the best agreement between the model prediction and the ChIP experiment was found for K_A=200 nM (Fig. 3B), corresponding to a condition of very moderate binding cooperativity between adjacent kB sites (N=-0.78 k_BT, much smaller than the interaction energies J and L that describe Pol II binding and recruitment, respectively).

15
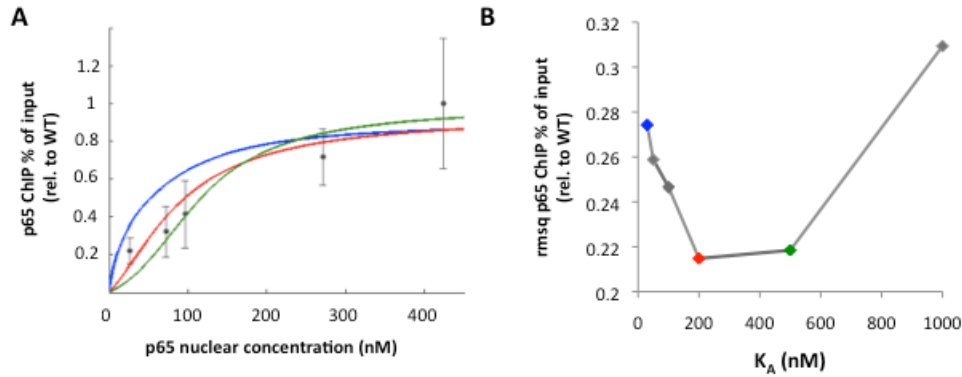
Figure 2. (A) Model 1 predictions vs. experimental data on the average kB site occupancy in the *NFKBIA* promoter. Average p65 occupancy (grey markers, mean ± Q-PCR error propagated from SD of technical replicates of a single representative experiment) was measured in ChIP in p65 knock-down clonal cell lines after 20 minutes TNF treatment and renormalized to the WT recruitment. NF-kB binding constant K_A was set to 30 nM (blue line), 200 nM (red line) and 500 nM (green line). Please refer to Table 1 for the parameter values associated with the different binding constants. Model predictions were rescaled by a multiplicative constant to be compared to the ChIP data, which was obtained by minimizing the root mean squares of the prediction vs. the experimental data. (B) The minimized root mean squares (model vs. ChIP data) are plotted as a function of the NF-kB binding constant K_A. Colored markers correspond to the three curves plotted in panel A. The best agreement is found for K_A=200 nM (red marker), corresponding to non-cooperative NF-kB binding.

To further characterize the validity of Model 1 in describing the operation of NF-kB dependent promoters, we selected three parameter sets among the ones listed in table 1, corresponding to NF-kB binding anti-cooperativity, moderate cooperativity (in the case of the best agreement between the model prediction and the induction of kB site occupancy on the *NFKBIA* promoter, K_A=200 nM) and stronger cooperativity. We then asked the model to predict the transcriptional induction profiles of other NF-kB target genes whose promoter regions contain less than six kB sites, including conserved and non-conserved sites (*TNFAIP3*, 4 sites; *NFKB1*, 3 sites; *NFKB2*, 5 sites; and *CSF1*, 4 sites). We rescaled the predictions of the model to the experimental data by a multiplicative constant that was found by minimizing the root mean square distances to the experimental points (Fig. 3).

Thus Model 1 is able to reproduce the correct induction of *NFKBIA* transcriptional activity and the average recruitment of NF-kB on the cluster in the *NFKBIA* promoter, and to recapitulate the transcriptional induction of other NF-kB target genes (although with a generally poor agreement to the experimental data). We will discuss in detail the quality of Model 1 predictions after discussing Model 3 below.

16
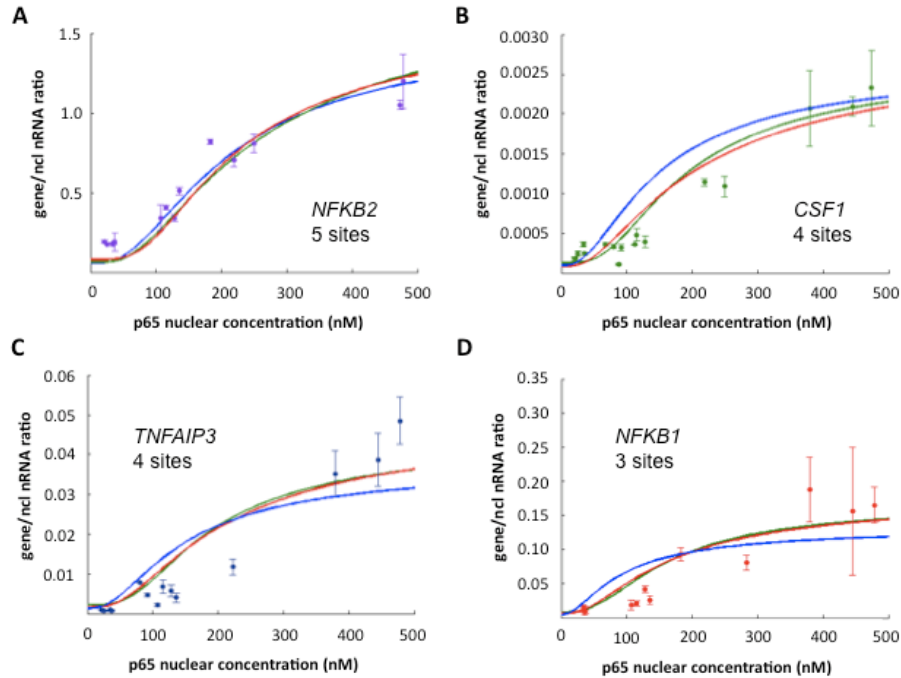
Figure 3. The predictions of Model 1 regarding the induction of genes with n<6 kB sites, obtained by setting K_A to 30 nM (bue line), 200 nM (red line) and 500 nM (green line) and using in each case the parameters extracted case in the fit of the *NFKBIA* induction profile. Model predictions were compared to the experimental data regarding (A) *NFKB2*, (B) *CSF1*, (C) *TNFAIP3* and (D) *NFKB1*.

Model 2. Non-additive Pol II recruitment

We next tested the possibility of fitting the *NFKBIA* transcriptional induction with the second variant of the model, wherein only one of the bound NF-kB molecules can interact with the Pol II complex, no matter how many TFs are bound to the promoter region.

We adopted the same strategy described above, and imposed different values of the NF-kB binding constant K_A. We obtained reasonable fits of the experimental data (rms<1 in units of *NFKBIA/ncl* nRNA ratio) only for K_A much higher than 500 nM and exceedingly distant to the experimental values (best fit with K_A=5000 nM, Fig. 4). Rms values similar to the ones obtained by fitting with model 1 were obtained only for K_A>1µM, thus for much weaker affinities as compared to the in vitro measured values. In the range of the observed in vitro binding affinities (K_A=20-300 nM), we obtained very poor fits to the data, due to the fact that the non-additive character of Pol II recruitment leads to an hyperbolical behavior of the curve in the low p65 regime, which does not reproduce the observed slightly sigmoidal response (Fig. 4A, blue curve).
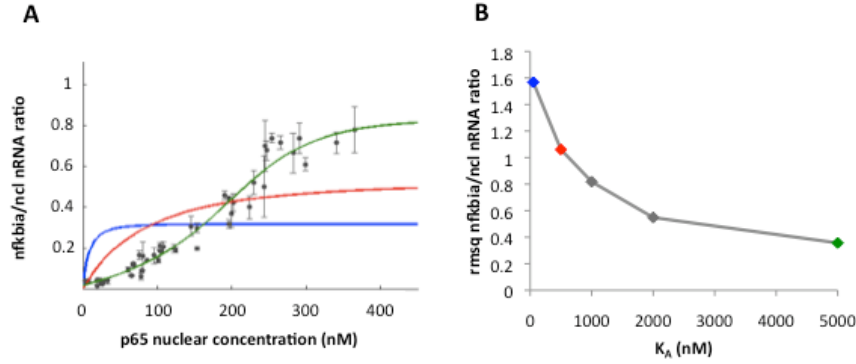
Figure 4. (A) Best fit of the *NFKBIA* induction profile with Model 2 with three representative values of the NF-kB binding constant. K_A was set to 50 nM (bue line), 500 nM (red line) and 5000 nM (green line). The correlation coefficients associated with this fit are r=0.458, r=0.845 and r=0.977, respectively. (B) Root mean squares of the fits obtained by imposing different values of K_A.

K_A (nM)	N	J	L	α	r (corr. coeff.)
50	22.683	23.8919	-15.3964	1558.23	0.457729
500	1.79983	14.471	-9.58674	69.978	0.8454636
1000	-0.855935	14.0466	-9.95832	37.1522	0.911995
2000	-1.8695	14.1059	-9.9077	49.0353	0.956934
5000	-2.98404	9.09434	-3.9711	140.825	0.977071
10000	-3.6149	4.36468	-4.39159	1.62814	0.977425

Table 2. Best estimates of the free parameters obtained by fitting the *NFKBIA* induction profiles with Model 2 for the various values of the NF-kB binding constants. Interaction parameters are expressed in units of k_BT. α and *r* stand for the multiplicative constant and the correlation coefficient, respectively.

We wondered whether the fact that we could fit the data in a regime of high K_A could reflect the real mechanism of operation of the promoter, despite the binding constants did not agree with the in vitro measured values. To this purpose, we compared the predictions of the model for the average kB site occupancy on the promoter of *NFKBIA* with the ChIP data already shown in Fig. 2. Since for high values of K_A a moderate extent of NF-kB binding cooperativity was required to adequately fit the *NFKBIA* induction profile (Table 2), the model prediction for p65 recruitment had a very poor agreement with the ChIP data (Fig. 5, red and green curves). Conversely, the ChIP data were best described when imposing lower K_A values (Fig. 5, blue line), which however correspond to very poor fits of the *NFKBIA* induction profile (Fig. 4A, blue line).

In summary, none of the identified fits of Model 2 describes *either* the *NFKBIA* transcriptional induction or p65 recruitment on the cluster, leading us to discard this mode of promoter operation.
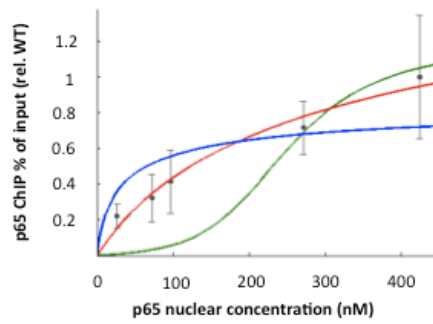
Figure 5. The predictions of Model 2 vs. the experimental data regarding p65 recruitment on the cluster of 6 binding sites in the *NFKBIA* promoter. The NF-kB binding constant K_A was set to 50 nM (blue), 500 nM (red) and 5000 nM (green). Please refer to Table 3 for the parameter values associated with the different binding constants. Model predictions were rescaled by a multiplicative constant to be compared to the ChIP data.

Model 3. Additive Pol II recruitment.

Finally, we fitted the experimental induction profile of *NFKBIA* with Model variant 3, wherein we suppose that every bound NF-kB can interact in an independent and additive fashion with the Pol II complex.

Again, we obtained adequate fits in the whole range of in vitro K_A (Fig. 6A). Since the quality of the fit increased with increasing K_A, we extended the range of affinities up to 2 μM. The quality of the fit reached a maximum (small root mean squares) in the very low affinity regime (high values of K_A, Fig. 6B). The correlation coefficients were similar to those obtained with Model 1.
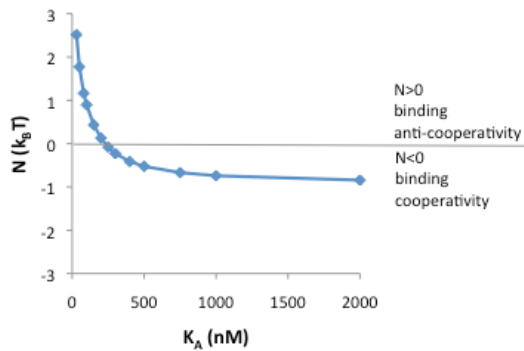
Notably, the best estimates of the cooperative binding energy (parameter N) were confined to a very small range when varying the value of K_A above 100 nM (Fig. 6). The data could in fact be fitted in the substantial absence of binding cooperativity (N between -0.5 and 0.5 k_BT) when K_A was in the range between 150 and 750 nM. For higher affinities (lower K_A), a moderate degree of binding anti-cooperativity was required to fit the data, while for high affinities NF-kB binding had be cooperative to obtain an adequate agreement (Table 3 and Fig. 7).
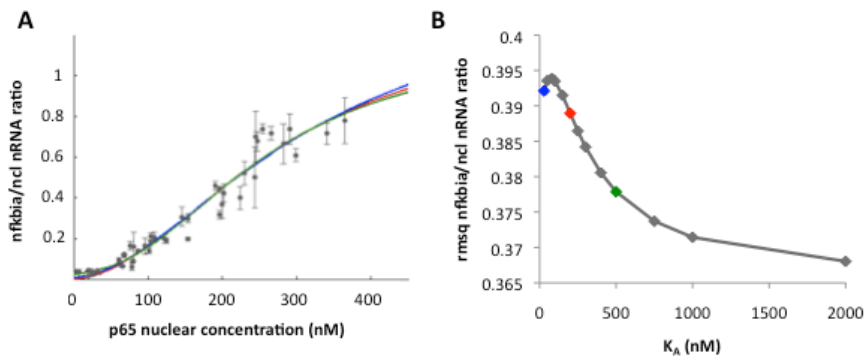
Figure 6. (A) Best fit of the *NFKBIA* induction profile with Model 3 with three representative values of the NF-kB binding constant. K_A was set to 30 nM (bue line), 200 nM (red line) and 500 nM (green line). The correlation coefficients associated with this fit are r=0.973, r=0.973 and r=0.974, respectively. (B) Root mean squares of the fits obtained by imposing different values of K_A.

K_A (nM)	N	J	L	α	r (corr. coeff.)
30	2.51568	14.5763	-3.8486	1.27279	0.972898
50	1.77315	11.1769	-2.84904	1.37084	0.972694
80	1.16329	8.76149	-2.13978	1.51481	0.972559
100	0.896246	7.83902	-1.86713	1.60572	0.972541
150	0.432357	6.49188	-1.45862	1.8144	0.97265
200	0.12803	5.77897	-1.24359	1.95547	0.972884
250	-0.0810666	5.43539	-1.12662	1.98127	0.973162
300	-0.228412	4.98784	-1.06473	1.90564	0.973435
400	-0.414794	4.49331	-1.02543	1.65092	0.973902
500	-0.524799	4.15746	-1.0381	1.43687	0.974257
750	-0.669084	3.69661	-1.13856	1.15915	0.974816
1000	-0.740904	3.48017	-1.26012	1.04612	0.975123
2000	-0.843459	3.21098	-1.69064	0.924395	0.975584

Table 3. Best estimates of the interaction parameters obtained by fitting the *NFKBIA* induction profiles with Model 3 for the various values of the NF-kB binding constants. Interaction parameters are expressed in units of $k_B T$. α and *r* stand for the multiplicative constant and the correlation coefficient, respectively.


Figure 7. The best estimates of the parameter N, setting the strength of NF-kB binding (anti-) cooperativity, are plotted as a function of the NF-kB binding constant K_A. The values of N are listed in Table 3, and were obtained in independent fits with fixed values of K_A.

We have seen so far that the data regarding *NFKBIA* induction could be adequately fitted by Model 3 in a wide range of affinities, leading (similarly to Model 1) to different estimates of the parameter setting the strength of NF-kB binding cooperativity. To determine which of the parameter combinations best described the actual mechanism of operation of the promoter, notably concerning NF-kB binding cooperativity, we used again the p65 ChIP experiment already shown in Figs. 2 and 4, describing p65 recruitment on the cluster as a function of p65 nuclear concentration. As in the case of Model 1, we asked the model to predict the average amount of NF-kB recruited to the six binding sites in the *NFKBIA* promoter, using each of the parameter sets determined in the fit of the *NFKBIA* transcriptional induction profile. Again, we rescaled each profile of NF-kB occupancy with an adequate multiplicative factor to compare it to the ChIP data, which we found by minimizing the root mean squares of the model prediction vs. the experimental data (Fig. 8A).

Importantly, the best agreement between the model prediction and the ChIP experiment was found for K_A=200 nM (Fig. 8B), corresponding to the second minimum absolute value of the parameter N (N=0.13 k_BT) among all parameter sets derived from the *NFKBIA* fit (Figure 9). The *NFKBIA* fit for this parameter set had an excellent agreement with the experimental data (rmsq= 0.388, r=0.973).

This shows that Model 2 is able to accurately fit the *NFKBIA* transcriptional induction profile, and to *predict* precisely the average NF-kB occupancy on the cluster of kB sites (more precisely than

Model 1, see below). The best parameter combination corresponds to a case wherein the NF-kB binding constant lies in the measured range (K_A=200 nM) and NF-kB binding to adjacent sites in the promoter is *not cooperative*.
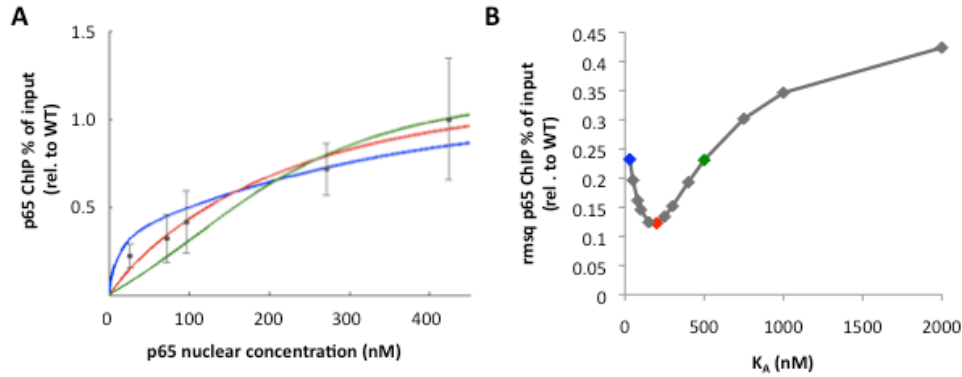

Figure 8. (A) Model predictions vs. experimental data regarding p65 recruitment on the cluster of 6 binding sites in the *NFKBIA* promoter. The NF-kB binding constant K_A was set to 30 nM (strong binding anti-cooperativity, blue), 200 nM (no binding cooperativity, red) and 500 nM (moderate cooperativity, green). Please refer to Table 3 for the parameter values associated with the different binding constants. Model predictions were rescaled by a multiplicative constant to be compared to the ChIP data, which was obtained by minimizing the root mean squares of the prediction vs. the experimental data. (B) The minimized root mean squares (model vs. ChIP data) are plotted as a function of the NF-kB binding constant K_A. Colored markers correspond to the three curves plotted in panel A. The best agreement was found for K_A=200 nM (red marker), corresponding to non-cooperative NF-kB binding.
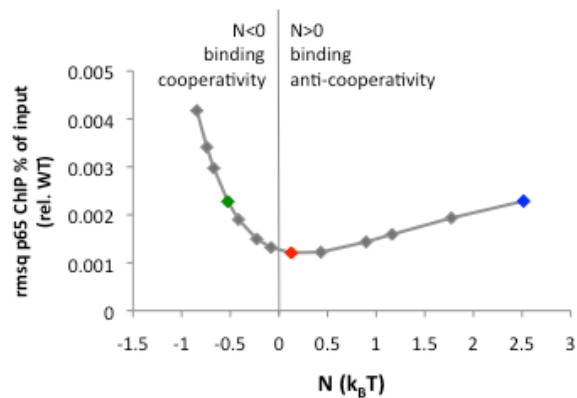
Figure 9. The minimized root mean squares (model prediction vs. ChIP data) are plotted as a function of the free energy of binding cooperativity (parameter N). Colors as in Figure 8.

To further characterize the consistency of this interpretation, we proceeded as in the case of Model 1 and we asked Model 3 to predict the transcriptional induction profiles of genes with n<6 kB sites in their promoters, imposing the parameter set that best recapitulates the *NFKBIA* data (K_A=200 nM, no binding cooperativity) and the two additional parameter sets already shown in Fig. 8A (corresponding to NF-kB binding cooperativity and anti-cooperativity). After rescaling the model output to the gene/*ncl* nRNA ratios by a multiplicative constant (found by minimizing the mean square roots of prediction vs. experimental data), we found a good agreement between the model predictions and the experimental profiles (Fig. 10).

21
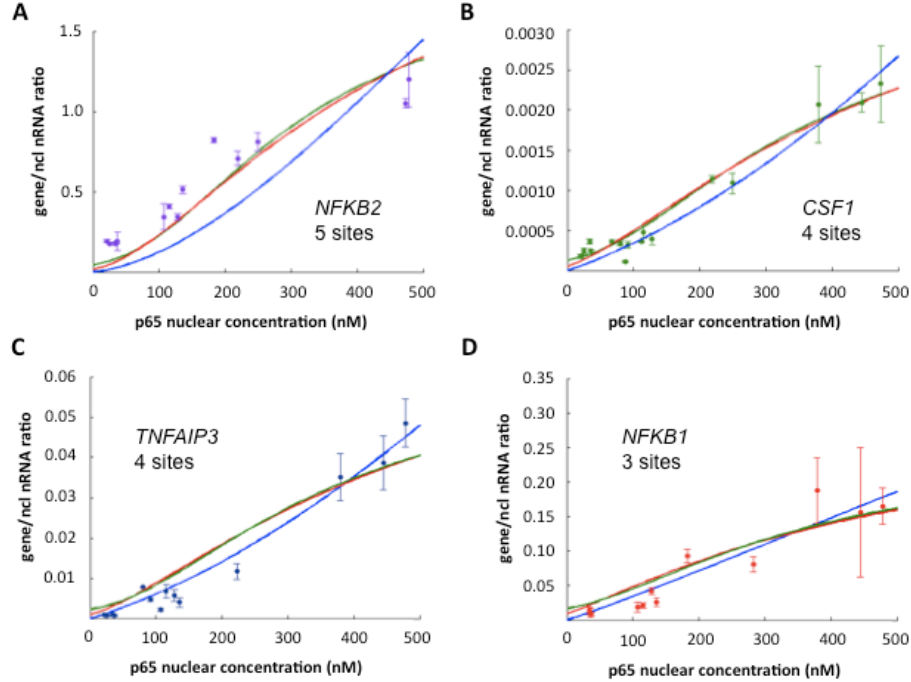
Figure 10. The predictions of Model 3 regarding the induction of genes with n<6 kB sites, obtained by setting K_A to 30 nM (bue line), 200 nM (red line) and 500 nM (green line) and using in each case the parameters extracted case in the fit of the *NFKBIA* induction profile. Model predictions were compared to the experimental data regarding (A) *NFKB2*, (B) *CSF1*, (C) *TNFAIP3* and (D) *NFKB1*.

Model 3 describes best the experimental observations.

Both Models 1 and 3 are able to reproduce (although to different extent) our experimental observations concerning the *NFKBIA* transcriptional induction, the average kB site occupancy in the *NFKBIA* promoter and the transcriptional induction of other NF-kB target genes with n<6 kB sites.

However, a careful analysis of the quality of fits and model predictions leads to the choice of Model 1 as the most representative of the actual operation mechanism of a NF-kB-dependent promoter.

Model 1, although providing accurate fits of the *NFKBIA* induction profile (almost as accurate as those obtained with Model 3 in terms of rmsq distances), is 50% less performing in predicting the average kB site occupancy with respect to Model 3 (Fig. 11A). The global quality of the predictions for the other NF-kB target genes is also sensitively lower in the case of Model 1 as compared to Model 3 (Figure 11B). With the only exception of *NFKB2* (maybe due to its higher basal level of transcription as compared to the other genes we characterized), Model 3 returned rmsq values between 20% and 70% lower than Model 1.

To quantify the goodness of agreement of the three different variants of the model with the experimental data, we exploited the capacity of our model to return not only the average values of Pol II occupancy on a gene with n kB sites ($<\sigma_0>$) and of the mean kB site occupancy ($<\sigma_i>$), but also their equilibrium fluctuations $\delta\sigma_0$ and $\delta\sigma_i$, respectively (see the Supplementary information on the thermodynamic model, Eq. (16)). Thus, given a model variant and a certain parameter set, the model returns outputs of the type $m \pm \Delta$, where m is the average value of the observable of interest ($<\sigma_0>$ or $<\sigma_i>$) and Δ is its associated statistical uncertainty ($\delta\sigma_0$ or $\delta\sigma_i$, respectively).

Supposing that m has a Gaussian distribution of width Δ, one can estimate the probability that model j (where j stands for variant 1, 2 or 3) returns *exactly* the measurement X (where X can be either the measured *NFKBIA* transcriptional activity, an average kB site occupancy, or the transcriptional activity of any other target gene at any given p65 concentration):

$$p(X \mid \mathrm{mod}\, j) = \frac{1}{\sqrt{2\pi\Delta}} \exp\left[-\frac{(X-m)^2}{2\Delta}\right].$$

Therefore, the probability of obtaining *exactly* the whole series of experimental measurements belonging to the dataset *{X}* (containing *NFKBIA* transcriptional activities, mean kB site occupancies and the transcriptional activities of the other target genes considered in the analysis) is given by

$$p(\{X\} \mid \mathrm{mod}\, j) = \prod_k \frac{1}{\sqrt{2\pi\Delta_k}} \exp\left[-\frac{(X_k-m_k)^2}{2\Delta_k}\right],$$

where *k* runs over all points of the dataset.

According to Bayes' theorem, the probability for model *j* (*j*=1,2,3) to be "correct" (assuming not to have any prior information on the validity of the three models) is given by

$$p(\mathrm{mod}\, j \mid \{X\}) = \frac{p(\{X\} \mid \mathrm{mod}\, j)}{p(\{X\} \mid \mathrm{mod}1) + p(\{X\} \mid \mathrm{mod}2) + p(\{X\} \mid \mathrm{mod}3)}.$$

We calculated the relative probabilities of each of the three model variants using the parameter sets that returned the best agreement with the profiles of kB site occupancy, and obtained the following results:

Model 1: p = 33.8%   (K_A=200 nM)
Model 2: p ≅ 0%   (K_A=500 nM)
Model 3: p = 66.1%   (K_A=200 nM),

which confirms that Model 3 gives the best interpretation of our experimental observations.
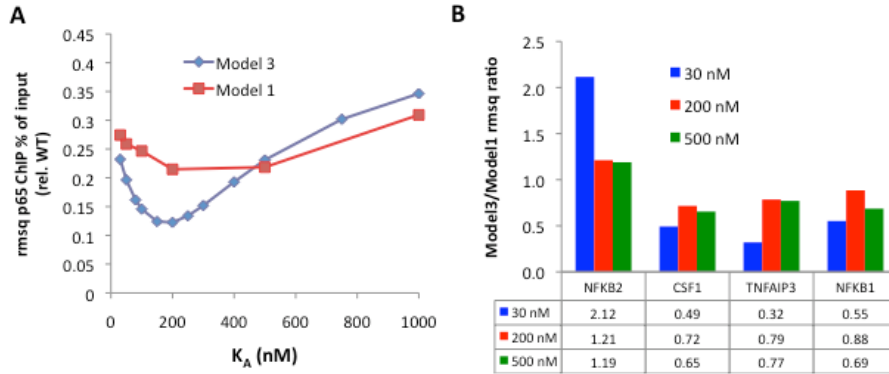
Figure 11. (A) The agreement of predictions of Model 1 and 3 with the ChIP data concerning the average kB site occupancy (see Figs. 2 and 4). Model 3 returns 50% better agreements with the experimental points (minimum rmsq=0.123 vs. 0.215 at K_A=200 nM). (B) The ratio between the rmsq values of Model 3 and Model 1 predictions for the induction profiles of NF-kB target genes with n<6 kB sites. Three different values of K_A were considered (colors as in Figs. 3 and 10). Model 3 generally returns better predictions as compared to Model 1 (Model3/Model1 rmsq ratio <1).

Conserved kB sites only.

We also performed the analysis of transcriptional induction profiles under the assumption that only kB sites that are conserved in more than half of the placental mammalian genomes contribute to NF-kB binding. Upon this assumption, the *NFKBIA* promoter contains *n=5* kB sites. The number of kB sites of the other target genes are listed in Table 1 in the manuscript.

As shown below, the results of the analysis performed including conserved and non-conserved sites do not change when including only conserved kB sites, although the parameter sets that best recapitulate the experimental observations are slightly different. Model 3 remains the most adequate to describe the mechanism of operation of *NFKBIA* both in terms of transcriptional induction and NF-kB recruitment to kB sites in the promoter, in conditions wherein NF-kB binding to adjacent kB sites is non-cooperative. We report hereafter an abbreviated description of this alternative analysis.

Model 1. All-or-none NF-kB-Pol II interaction.

Similarly to the previous analysis, Model 1 could fit the *NFKBIA* transcriptional induction profile in a wide range of NF-kB binding affinities (Fig. 12). Among all parameter sets, the best agreement between the model prediction for the average kB site occupancy and the p65 ChIP data was found for $K_A=100$ nM (Fig. 13), corresponding to non-cooperative NF-kB binding (N=0.2 k_BT).
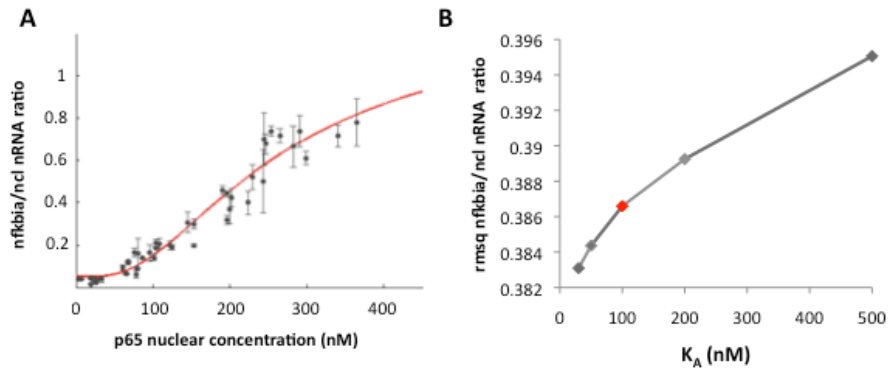
Figure 12. (A) Best fit of the *NFKBIA* induction profile with Model 1 obtained by imposing $K_A=100$ nM and under the hypothesis that the promoter region contains n=5 kB sites. The correlation coefficient associated with this fit is r=0.973. (B) Root mean squares of the various fits obtained by imposing different values of K_A and n=5.

24
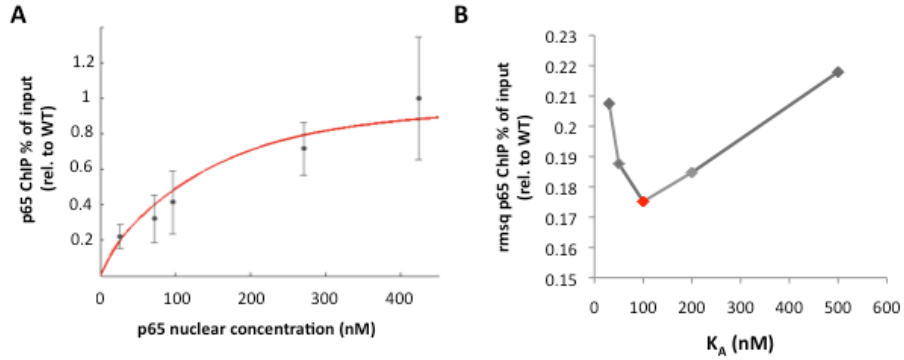
Figure 13. (A) Model 1 predictions vs. experimental data on the average kB site occupancy in the *NFKBIA* promoter. Average p65 occupancy (grey markers, mean ± Q-PCR error propagated from SD of technical replicates of a single representative experiment) was measured in ChIP in p65 knock-down clonal cell lines after 20 minutes TNF treatment and renormalized to the WT recruitment. NF-kB binding constant K_A was set to 100 nM (red lineModel predictions were rescaled by a multiplicative constant to be compared to the ChIP data, which was obtained by minimizing the root mean squares of the prediction vs. the experimental data. (B) The minimized root mean squares (model vs. ChIP data) are plotted as a function of the NF-kB binding constant K_A. The best agreement (rmsq=0.175) is found for K_A=100 nM (red marker), corresponding to non-cooperative NF-kB binding.

Model 2. Non-additive Pol II recruitment

As in the analysis that included conserved and non-conserved sites, Model 2 only returned acceptable fits of the *NFKBIA* transcriptional induction profile for much higher binding affinities as compared to experimental values (best fit for K_A=5000 nM, Fig. 14B). Again, good fits of the *NFKBIA* induction profiles corresponded to parameter sets returning very poor agreements with the p65 ChIP recruitment profile, and vice versa (Fig. 15). Thus, again, we rejected Model 2 as a mode of promoter operation.
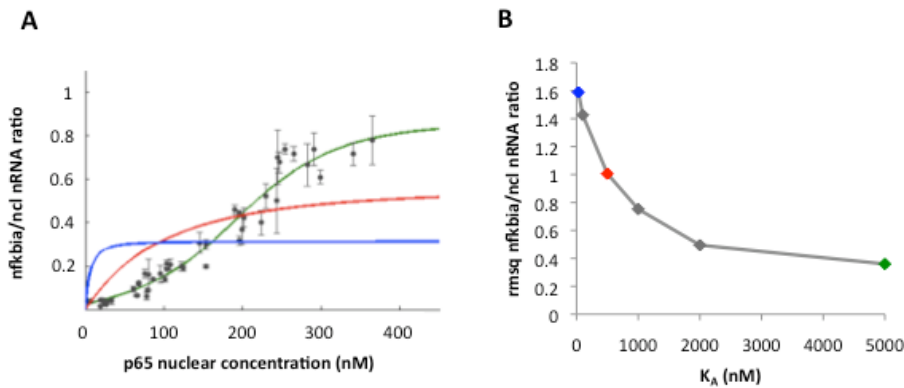
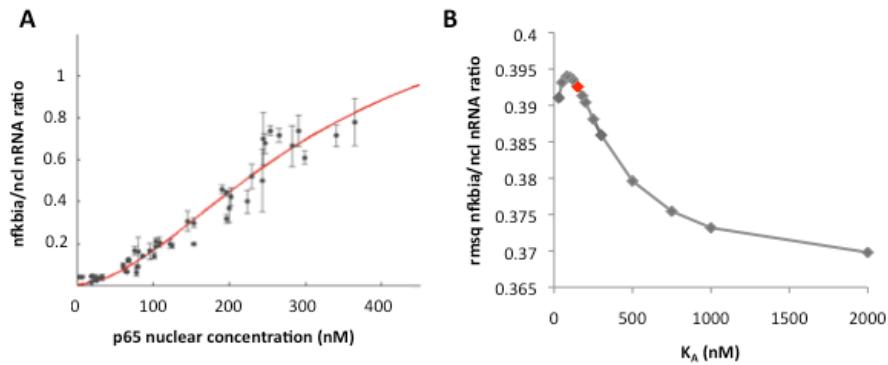**Figure 14.** (A) Best fit of the *NFKBIA* induction profile with Model 2 with three representative values of the NF-kB binding constant and n=5. K_A was set to 30 nM (bue line), 500 nM (red line) and 5000 nM (green line). (B) Root mean squares of the fits obtained by imposing different values of K_A.
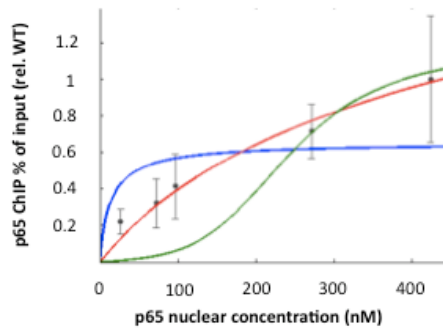
Figure 15. The predictions of Model 2 vs. the experimental data regarding p65 recruitment on the cluster of 5 binding sites in the *NFKBIA* promoter. The NF-kB binding constant K_A was set to 50 nM (blue), 500 nM (red) and 5000 nM (green). Please refer to Table 3 for the parameter values associated with the different binding constants. Model predictions were rescaled by a multiplicative constant to be compared to the ChIP data.

Model 3. Additive Pol II recruitment.

As in the previous analysis, also for n=5 Model 3 returned good fits in the whole range of experimental values of K_A (Fig. 16). The values of parameter N, controlling the strength of the cooperativity in NF-kB binding, were again found to be confined to the non-cooperative regime (N between -0.5 and 0.5 k_BT) for $K_A > 100$ nM (Fig. 17).

Figure 16. (A) Best fit of the *NFKBIA* induction profile with Model 3 when K_A was set to 150 nM (red line) and n=5. The correlation coefficient associated with this fit is r=0.973 and r=0.974, respectively. (B) Root mean squares of the fits obtained by imposing different values of K_A.
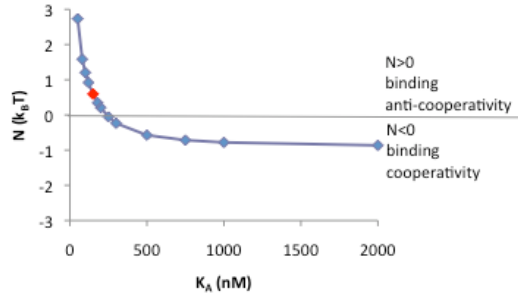
Figure 17. The best estimates of the parameter N, setting the strength of NF-kB binding (anti-) cooperativity, are plotted as a function of the NF-kB binding constant K_A. Red marker: K_A=150 nM, best agreement with p65 ChIP data.

When compared to the p65 ChIP data, the model returned the best agreement for K_A=150 nM, where N=0.59 k_BT (Fig. 18). Thus, also in the case wherein the *NFKBIA* promoter is supposed to contain 5 functional kB sites, Model 3 was found to best describe the operation of the *NFKBIA* promoter when K_A lies in the experimentally determined range and in a regime of substantially non-cooperative NF-kB binding to adjacent kB sites.

When applying the Bayesian formalism to the calculation of probabilities that each model returned the measured experimental data, we found the following results:

Model 1: p = 36.8% (K_A=100 nM)
Model 2: p $\cong$ 0% (K_A=500 nM)
Model 3: p = 63.1% (K_A=150 nM),

which confirms that Model 3, in the absence of NF-kB binding cooperativity, gives the best interpretation of our experimental observations also when only conserved kB sites are included into the analysis.
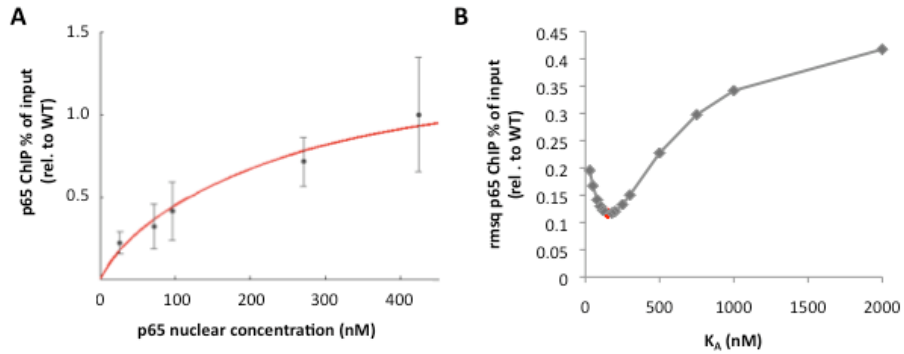
Figure 18. (A) Model predictions vs. experimental data regarding p65 recruitment on the cluster of 5 binding sites in the *NFKBIA* promoter. The NF-kB binding constant K_A was set to 150 nM (no binding cooperativity, red) Model predictions were rescaled by a multiplicative constant to be compared to the ChIP data, which was obtained by minimizing the root mean squares of the prediction vs. the experimental data. (B) The minimized root mean squares (model vs. ChIP data) are plotted as a function of the NF-kB binding constant K_A. The best agreement (rmsq=0.117) is found for K_A=150 nM (red marker), corresponding to non-cooperative NF-kB binding (N=0.59 k_BT).

SUPPLEMENTAL REFERENCES

[1] Grünwald, D., *et al* (2008). Probing intranuclear environments at the single-molecule level. Biophys J 94, 2847-2858.

[2] Fusco, A.J., Huang, D.B., Miller, D., Wang, V.Y., Vu, D., and Ghosh, G. (2009). NF-kappaB p52:RelB heterodimer recognizes two classes of kappaB sites with two distinct modes. EMBO Rep 10, 152-159.

[3] Phelps, C.B., Sengchanthalangsy, L.L., Malek, S., and Ghosh, G. (2000). Mechanism of kappa B DNA binding by Rel/NF-kappa B dimers. J Biol Chem 275, 24392-24399.

[4] Marquardt D. (1963). An Algorithm for Least-Squares Estimation of Nonlinear Parameters. SIAM Journal on Applied Mathematics 11: 431–441.

Thermodynamic model of NF-kB-dependent promoter operation

Introduction

We developed a model of NF-kB -dependent transcriptional activation that combines a purposely simple picture of promoter operation with strong experimental grounding regarding the *in vivo* dynamics of NF-kB and RNA polymerase II (Pol II).

The main focus of the model is calculating the probability of a Pol II complex to be active on a NF-kB target promoter as a function of the nuclear concentration of NF-kB, once that a specific hypothesis concerning the rules governing the *cis*-regulatory element (CRE) has been postulated. We consider the case of the CRE of a generic NF-kB target gene, where n binding sites are located. We will discuss the simplified case in which only one class of NF-kB dimers act on the CRE of interest (i.e. p65/p50 heterodimers, accounting for most NF-kB activity in non-immune cells [1]).

Let $[A(t)]$ be the NF-kB nuclear concentration at any given time t. In non-stimulated cells, $[A(t)] \simeq 0$, since nearly all NF-kB molecules reside in the cytoplasm. Upon stimulation with TNFα, $[A(t)]$ increases with time and reaches a maximum within 15-30 minutes, depending on the cell type, then decreases on similar timescales due to NF-kB-directed resynthesis of its inhibitor IkBα.

Let $[P]$ be the concentration of RNA polymerase II transcription preinitiation complexes (considered here as holoenzymes and denoted generically by Pol II) in the nucleus. We shall assume that $[P]$ is a constant in time.

We will describe the promoter in the context of **equilibrium thermodynamics**, assuming that:

1. NF-kB molecules and their n binding sites on the CRE are in a kinetic equilibrium at any given time t;

2. Pol II complexes are at equilibrium with the promoter.

The validity of these assumptions is ensured by the data reported in the manuscript and by published results [2, 3], which show that the nuclear NF-kB concentration varies on considerably longer timescales as compared to NF-kB exchange on DNA specific binding sites, to Pol II exchange at the promoter and to the timescale of transcriptional initiation. Thus, we will take

$$[A(t)] = [A] \tag{1}$$

where $[A]$ denotes the average nuclear concentration of NF-kB. We will treat the problem in the **canonical ensemble** of classical statistical mechanics, the cell population providing the statistical ensemble of replicas of the system.

Formalism

We consider the general case of a NF-kB target gene whose CRE contains n *identical* NF-kB binding sites. Of course this is an oversimplified view of a real promoter region containing binding sites with different sequences and affinities for the various NF-kB dimers. Each of our 'model' binding sites may represent an average over the 'real' n sites, and has an equilibrium *in vivo* binding constant K_A for NF-kB dimers. Let K_P be the binding constant of Pol II for the core promoter sequence.

The n binding sites sites in the promoter region can be treated similarly to a **one-dimensional Ising chain** [4] with n 'spin' variables σ_i (Figure 1). Define the value of σ_i as the occupancy of binding site i:

- $\sigma_i = 0$ if the i-th site is non-occupied

- $\sigma_i = 1$ if the i-th site is occupied.

The Pol II docking site may be regarded as an additional spin σ_0. If NF-kB binding is non-cooperative, the $n+1$ spin variables are independent, and the free energy of each configuration of the system can be written as

$$H_0 = K \sum_{i=1}^{n} \sigma_i + J \sigma_0 \tag{2}$$

where K and J are the single-molecule binding free energies of NF-kB and Pol II, respectively, to their binding sites. K and J are related to the concentrations and the binding constants by the following relationships:

$$K = -kT \log \frac{[A]}{K_A}, \tag{3}$$

$$J = -kT \log \frac{[P]}{K_P}. \tag{4}$$

If instead the binding of NF-kB to adjacent DNA binding sites is cooperative, an additional term enters the expression due to the fact that there is a further change in free energy if NF-kB binds to a site whose 5' or 3' neighbour site is already occupied. This latter term is equivalent to a first-neighbour interaction in the classical Ising model:

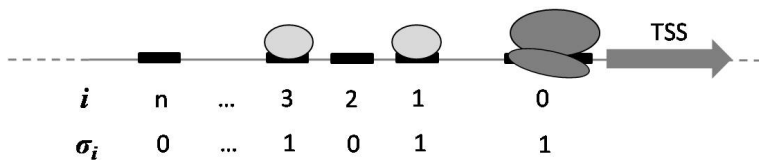$$H_{coop} = N \sum_{i=1}^{n-1} \sigma_i \sigma_{i+1} \tag{5}$$

Figure 1: Schematics of the promoter model. In the depicted situation, binding sites 1 and 3 are bound by NF-kB dimers (light gray circles): thus, $\sigma_1 = \sigma_3 = 1$ while $\sigma_2 = \sigma_4 = ... = \sigma_n = 0$. $\sigma_0 = 1$ since Pol II is bound to the core promoter.

where N is an interaction constant that sets the strength of the coupling between adjacent binding sites. $N < 0$ corresponds to NF-kB cooperative binding, as binding to adjacent sites is ergetically favorable. Conversely, if $N > 0$, binding to adjacent sites is energetically unfavorable (anti-cooperative binding). The case $N = 0$ NF-kB corresponds to non-cooperative binding.

How the n binding sites are used to recruit Pol II to the trasncription start site depends explicitly on an *a priori* hypothesis concerning the logic underlying promoter operation. This enters the model via an interaction term $L \cdot H_{int}$ that describes the effective interaction between bound NF-kB molecules and Pol II. Being NF-kB a transcriptional activator, we set the coupling constant $L < 0$. We suppose that bound NF-kB interacts with Pol II via an effective interaction (whose strength is set by the parameter L) that renormalizes the interactions with all intermediate adapters between the two (e.g. mediator complexes etc).

We formulated three different hypotheses, reflecting three alternative logics of promoter operation.

1. **All-or-none Pol II recruitment**. Pol II interacts with bound NF-kB only when all n sites are bound simultaneously:

$$H_{int} = \sigma_0 \prod_{i=1}^{n} \sigma_i. \tag{6}$$

Note that H_{int} is always equal to zero, unless all NF-kB binding sites and the Pol II are bound ($\sigma_i = +1$ for $i = 0...n$).

This would result in limiting the activation of genes with many sites, which would require TF concentrations high enough to saturate all binding sites in the cluster for transcription to be activated. Although counterintuitive at first, this mode of operation might ensure for instance that kBα, which is the negative feedback of the NF-kB pathway, is not induced before a given nuclear concentration of NF-kB is reached, thus preventing a premature shut-off of the response.

2. **Non-additive Pol II recruitment**. Pol II interacts only with only one NF-kB molecule bound to the CRE, no matter how many other are bound:

$$H_{int} = \sigma_0 \left[1 - \prod_{i=1}^{n} (1 - \sigma_i) \right]. \tag{7}$$
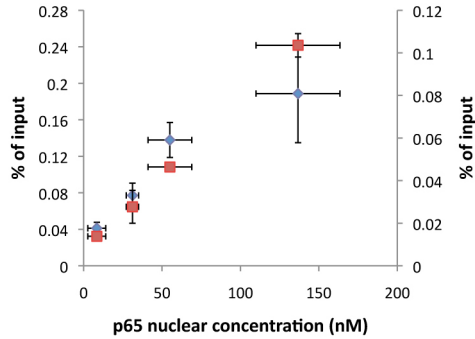
Figure 2: The number of elongating Pol II is proportional to the number of Pol II that are recruited to the promoter of *nfkbia*. The plot shows the results of anti-Pol II ChIP, wherein the immunoprecipitated DNA was amplified using promoter-specific primers (blue marks, left vertical axis) and primers amplifying a region between intron 3 and exon 4 (red marks, right vertical axis). ChIP experiments were performed in different HCT116 p65 knock-down clonal cell lines stimulated with 30 min TNFα, each cell line expressing differential amounts of residual p65.

Upon this assumption, the role of a cluster would be to increase the probability that NF-kB and Pol II interact, but not the overall stregth of the interaction.

3. **Additive Pol II recruitment**. Each bound NF-kB interacts with Pol II in an additive fashion:

$$H_{int} = \sigma_0 \sum_{i=1}^{n} \sigma_i \tag{8}$$

The role of a cluster of binding sites would be thus to promote stronger and stronger NF-kB-Pol II interactions as the number of binding sites increases.

The complete expression of the free energy of the promoter is thus given by

$$H_{tot} = H_0 + H_{int} + H_{coop}. \tag{9}$$

We suppose that the number of Pol II that enter an elongating state is a fixed fraction ($\simeq 1\%$, see Ref. [3]) of the number of Pol II that have been recruited to the promoter. This is supported by the ChIP data shown in Figure 2, which prove that the number of elongating ('active') Pol II are proportional to

the number of Pol II detected on the promoter of *nfkbia*, both increasing mono-
tonically with increasing nuclear concentration of NF-kB. Thus, our estimate of
the trancriptional activity of the gene will be the **average Pol II occupancy**
on the core promoter, up to a multiplicative factor α:

$$P_{active} = \alpha \langle \sigma_0 \rangle, \tag{10}$$

that is the conditional probability of activating the transcription if the polimerase
is bound. Here $\langle ... \rangle$ represents a Boltzmann-weighted average over all the possi-
ble realizations of the system. Please note that P_{active} is a well-defined observ-
able, since we challenge the predictions of the model by detecting the population-
averaged number of nascent RNAs over populations of millions of cells, providing
the statistical ensemble of replicas of the system.

To calculate $\langle \sigma_0 \rangle$, we proceed as follows. First, we compute the partition
function of the promoter, defined as the sum of the Boltzmann factors of all
possible configurations of the system:

$$Z = \sum_{\{\sigma\}} \exp\left[-\beta(H_0\{\sigma\} + H_{int}\{\sigma\} + H_{coop}\{\sigma\})\right] \tag{11}$$

where $\beta = 1/k_B T$ and $\{\sigma\}$ reresents all possible configurations of the $n + 1$
'spin' variables. We then calculate the average free energy of the system,

$$F = -\frac{1}{\beta} \ln Z, \tag{12}$$

and finally calculate σ_0 as the derivative of F with respect to the single-molecule
Pol II binding energy J:

$$\langle \sigma_0 \rangle = \frac{\partial F}{\partial J}. \tag{13}$$

The same procedure can be used to calculate the mean NF-kB occupancy of
any (say the i-th) site in the cluster:

$$\langle \sigma_i \rangle = \frac{1}{n} \frac{\partial F}{\partial K}. \tag{14}$$

The second derivative of F with respect to the parameter J leads the quadratic
variance of the Pol II occupancy $\langle \sigma_0 \rangle$:

$$\langle \sigma_0^2 \rangle - \langle \sigma_0 \rangle^2 = -\frac{1}{\beta} \frac{\partial^2 F}{\partial J^2}. \tag{15}$$

Given a certain value of the NF-kB concentration $[A]$, the square root of Eq. (15)
gives the width of the distribution of Pol II occupancy over the cell population,
and hence the intrinsic component of the transcriptional noise [5]:

$$\delta\sigma_0 = \sqrt{-\frac{1}{\beta} \frac{\partial^2 F}{\partial J^2}}. \tag{16}$$

Both Eqs. (13), (14) and (16) can be evaluated analytically by way of the
transfer matrix formalism of the 1D Ising model (see below).

Model 1. All-or-none Pol II recruitment

Suppose that Pol II interacts with TFs bound to the binding sites in the CRE only if *all* the n binding sites are simultaneously occupied. This corresponds to the following interaction term:

$$H_{int} = \sigma_0 \prod_{i=1}^{n} \sigma_i. \tag{17}$$

The complete expression of the free energy of any promoter configuration is then given by

$$H = K \sum_{i=1}^{n} \sigma_i + J \sigma_0 + L\sigma_0 \prod_{i=1}^{n} \sigma_i + N \sum_{i=1}^{n-1} \sigma_i \sigma_{i+1}. \tag{18}$$

To calculate the partition function explicitly, we isolate the contribution from $\sigma_i = 1$ for $i = 0...n$:

$$
\begin{aligned}
Z \;=\; & \sum_{\{\sigma\}\backslash\{1...1\}} e^{-\beta\left[K\sum_{i=1}^{n}\sigma_i + J\sigma_0 + N\sum_{i=1}^{n-1}\sigma_i\sigma_{i+1}\right]} \\
+ \;& e^{-\beta[nK+J+L+(n-1)N]} + e^{-\beta[nK+J+(n-1)N]} \\
- \;& e^{-\beta[nK+J+(n-1)N]}.
\end{aligned}
$$

The 'promoter' part of the partition function (the one concerning $\sigma_1 ... \sigma_n$) is formally equivalent to a one-dimensional Ising model with an applied external field K:

$$
\begin{aligned}
Z \;=\; & \left(1+e^{-\beta J}\right) \sum_{\sigma_1...\sigma_n} e^{-\beta\left[\frac{K}{2}\sum_{i=1}^{n}(\sigma_i+\sigma_{i+1})+N\sum_{i=1}^{n}\sigma_i\sigma_{i+1}\right]} \\
+ \;& e^{-\beta[nK+J+L+(n-1)N]} - e^{-\beta[nK+J+(n-1)N]}
\end{aligned}
$$

(where $\sigma_{n+1} = \sigma_1$). We apply the transfer matrix formalism [4] and re-write as follows:

$$\sum_{\sigma_1...\sigma_n} e^{-\beta\left[\frac{K}{2}\sum_{i=1}^{n}(\sigma_i+\sigma_{i+1})+N\sum_{i=1}^{n}\sigma_i\sigma_{i+1}\right]} = \mathrm{Tr}(M_1^n) \tag{19}$$

where

$$M_1 = \begin{pmatrix} e^{-\beta(K+N)} & e^{-\beta K/2} \\ e^{-\beta K/2} & 1 \end{pmatrix}. \tag{20}$$

Thus

$$
\begin{aligned}
Z \;=\; & \left(1+e^{-\beta J}\right)\mathrm{Tr}(M_1^n) \\
+ \;& e^{-\beta[nK+J+L+(n-1)N]} - e^{-\beta[nK+J+(n-1)N]}.
\end{aligned} \tag{21}
$$

By using the fact that $\partial \mathrm{Tr}(M_1)/\partial J = 0$, we can easily calculate $\partial \ln Z / \partial J$ and therefore $\langle \sigma_0 \rangle$. This latter can be cast in the form

$$\langle \sigma_0 \rangle = \frac{1}{1 + \frac{1}{F_{reg}^{(1)}} e^{\beta J}} \tag{22}$$
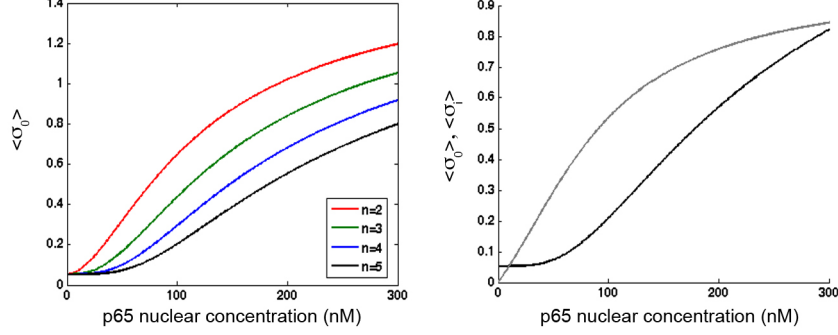
Figure 3: Left: The probability of having an active Pol II at the promoter as a function of NF-kB nuclear concentration for genes regulated by $n = 2 \div 5$ binding sites according to **Model 1**. Parameters were chosen within the best fits of the experimental data of *nfkbia* transcriptional activation (see the supplementary Analysis and fitting of transcriptional induction profiles): $K_A = 200$ nM, $N = -0.8\,k_BT$, $J = 6.7\,k_BT$, $L = -4.2\,k_BT$. Right: The average NF-kB binding site occupancy $\langle \sigma_i \rangle / n$ (grey line) and the average Pol II occupancy on the promoter $\langle \sigma_0 \rangle$ (black line) are plotted for a gene with 5 sites with the same parameter set.

where

$$F_{reg}^{(1)} = \frac{\text{Tr}(M_1^n) + e^{-\beta n K}e^{-\beta L}e^{-\beta(n-1)N} - e^{-\beta n K}e^{-\beta(n-1)N}}{\text{Tr}(M_1^n)}. \qquad (23)$$

By recalling Eqs. (3) and (4) and that $\langle \sigma_0 \rangle$ reflects the probability of activating transcription, we can write

$$P_{active}([A], n) = \alpha \, \frac{1}{1 + \frac{1}{F_{reg}^{(1)}([A],n)} \frac{K_P}{[P]}}. \qquad (24)$$

As in Ref. [6], the 'regulation function' $F_{reg}^{(1)}$ contains all the contributions from NF-kB binding and interaction with Pol II. If the nuclear concentration of NF-kB is set to zero ($[A] = 0$), then $F_{reg}^{(1)} = 1$ and Eq. (38) reduces to

$$P_{active}([A] = 0, n) = \alpha \frac{1}{1 + \frac{K_P}{[P]}}, \qquad (25)$$

which describes Pol II binding to the core promoter in the absence of NF-kB regulation and hence the basal level of transcription of the gene.

Whenever $[A] > 0$, then $F_{reg}^{(1)} > 1$ (Figure 3) and $K_P/F_{reg}^{(1)} < K_P$. Thus the net effect of NF-kB binding to the promoter and NF-kB-Pol II interactions is to increase the effective affinity of Pol II to the core promoter.

The average NF-kB occupancy of a single binding site can be calculated similarly by taking the derivative of Eq. (21) with respect to the parameter K (see Eq. (14)).

An example of the predictions of Model 1 for the transcriptional induction profiles ($\langle\sigma_0\rangle$ vs. $[A]$) and the NF-kB occupancy ($\langle\sigma_i\rangle$ vs. $[A]$) are shown in Figure 3.

Model 2. Non-additive Pol II recruitment

Suppose that, whatever the number of NF-kB molecules bound to the CRE, Pol II can interact with *only one* of them that. Supose that the energy of the system is then decreased by an amount $L < 0$. In this context, the role of the additional binding sites is to increase the probability of having one of these activating events, rather than to increase the overall NF-kB-Pol II interaction energy.

In this case, the free energy of the promoter is given by

$$H = K \sum_{i=1}^{n} \sigma_i + J\,\sigma_0 + L\,\sigma_0 \left[1 - \prod_{i=1}^{n}(1-\sigma_i) \right] + N \sum_{i=1}^{n-1} \sigma_i\sigma_{i+1}. \qquad (26)$$

The partition function can be calculated again by separating the contributions from $\sigma_0 = 0$ and $\sigma_0 = 1$,

$$
\begin{aligned}
Z &= \sum_{\sigma_1...\sigma_n} e^{-\beta\left[K\sum_{i=1}^{n}\sigma_i + N\sum_{i=1}^{n-1}\sigma_i\sigma_{i+1}\right]} \\
&+ \sum_{\sigma_1...\sigma_n} e^{-\beta\left[K\sum_{i=1}^{n}\sigma_i + (J+L) - L\prod_{i=1}^{n}(1-\sigma_i) + N\sum_{i=1}^{n-1}\sigma_i\sigma_{i+1}\right]}. \qquad (27)
\end{aligned}
$$

This expression can be simplified by noting that $\prod_{i=1}^{n}(1-\sigma_i) = 0$ whenever $\{\sigma_1...\sigma_n\} \neq \{0...0\}$, and isolating the contribution from this term:

$$
\begin{aligned}
Z &= \mathrm{Tr}(M_1^n) + e^{-\beta J} + e^{-\beta(J+L)}\left[\sum_{\sigma_1...\sigma_n} e^{-\beta\left[K\sum_{i=1}^{n}\sigma_i + N\sum_{i=1}^{n-1}\sigma_i\sigma_{i+1}\right]} - 1 \right] \\
&= \mathrm{Tr}(M_1^n) + e^{-\beta J} + e^{-\beta(J+L)}\left[\mathrm{Tr}(M_1^n) - 1\right]. \qquad (28)
\end{aligned}
$$

As usual, $\langle\sigma_0\rangle$ can be reduced to the form

$$\langle\sigma_0\rangle = \frac{1}{1 + \frac{1}{F_{reg}^{(2)}}e^{\beta J}} \qquad (29)$$

where now

$$F_{reg}^{(2)} = \frac{\mathrm{Tr}(M_1^n)e^{-\beta L} + 1 - e^{-\beta L}}{\mathrm{Tr}(M_1^n)}. \qquad (30)$$

Thus

$$P_{active}([A], n) = \alpha\,\frac{1}{1 + \frac{1}{F_{reg}^{(2)}([A],n)}\frac{K_P}{[P]}}. \qquad (31)$$

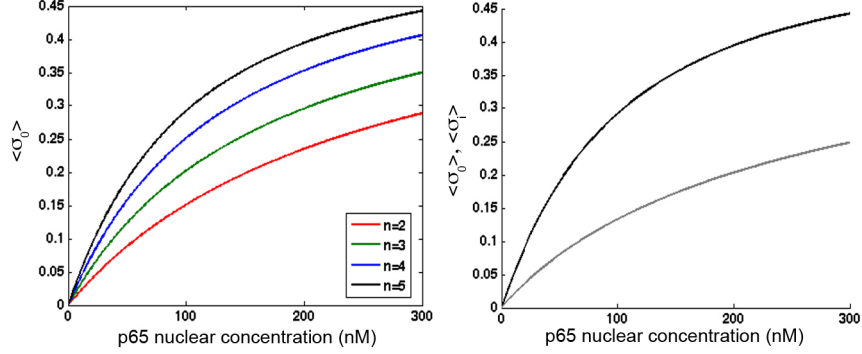See Figure 4 for an example of the predictions of Model 2.

Figure 4: Left: The probability of having an active Pol II at the promoter as a function of NF-kB nuclear concentration for genes regulated by $n = 2 \div 5$ binding sites according to **Model 2**. Parameters were chosen within the best fits of the experimental data of *nfkbia* transcriptional activation (see the supplementary Analysis and fitting of transcriptional induction profiles): $K_A = 500$ nM, $N = 1.8\,k_B T$, $J = 14.5\,k_B T$, $L = -9.6\,k_B T$. Right: The average NF-kB binding site occupancy $\langle \sigma_i \rangle / n$ (grey line) and the average Pol II occupancy on the promoter $\langle \sigma_0 \rangle$ (black line, rescaled by a numerical constant) are plotted for a gene with 5 sites with the same parameter set.

Model 3. Additive Pol II recruitment

Let *each* NF-kB molecule, once it is bound to any of the n binding sites in the CRE, interact with a Pol II complex. Suppose that the net effect of each of these interaction events is to lower the free energy of the system by an amount $L < 0$.

The complete Hamiltonian is

$$H = K \sum_{i=1}^{n} \sigma_i + J\,\sigma_0 + L\,\sigma_0 \sum_{i=1}^{n} \sigma_i + N \sum_{i=1}^{n-1} \sigma_i \sigma_{i+1}. \tag{32}$$

To calculate the partition function, we separate explicitly the contributions from $\sigma_0 = 0$ and $\sigma_0 = 1$:

$$
\begin{aligned}
Z \;=\; & \sum_{\sigma_1 \ldots \sigma_n} e^{-\beta \left[K \sum_{i=1}^{n} \sigma_i + N \sum_{i=1}^{n-1} \sigma_i \sigma_{i+1} \right]} \;+ \\
& + \sum_{\sigma_1 \ldots \sigma_n} e^{-\beta \left[K \sum_{i=1}^{n} \sigma_i + J + L \sum_{i=1}^{n} \sigma_i + N \sum_{i=1}^{n-1} \sigma_i \sigma_{i+1} \right]}.
\end{aligned}
\tag{33}
$$

This can be written as

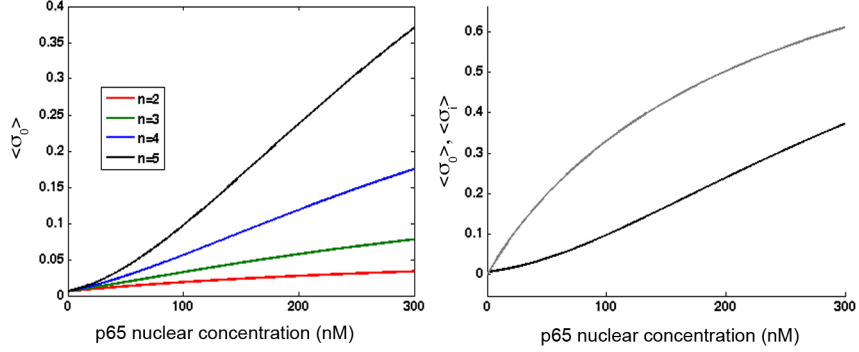$$Z = \mathrm{Tr}(M_1^n) + \mathrm{Tr}(M_2^n)\,e^{-\beta J} \tag{34}$$

Figure 5: Left: The probability of having an active Pol II at the promoter as a function of NF-kB nuclear concentration for genes regulated by $n = 2 \div 5$ binding sites according to **Model 3**. Parameters were chosen within the best fits of the experimental data of *nfkbia* transcriptional activation (see the supplementary Analysis and fitting of transcriptional induction profiles): $K_A = 200$ nM, $N = 0.1\,k_B T$, $J = 5.8\,k_B T$, $L = -1.3\,k_B T$. Right: The average NF-kB binding site occupancy $\langle \sigma_i \rangle / n$ (grey line) and the average Pol II occupancy on the promoter $\langle \sigma_0 \rangle$ (black line) are plotted for a gene with 5 sites with the same parameter set.

where the transfer matrix M_1 has introduced in Eq. (40), and

$$M_2 = \begin{pmatrix} e^{-\beta(K+L+N)} & e^{-\beta(K+L)/2} \\ e^{-\beta(K+L)/2} & 1 \end{pmatrix} \tag{35}$$

Again, by using the fact that $\partial \mathrm{Tr}(M_{1,2})/\partial J = 0$, one can reduce $\langle \sigma_0 \rangle$ to the form

$$\langle \sigma_0 \rangle = \frac{1}{1 + \frac{1}{F_{reg}^{(3)}} e^{\beta J}}, \tag{36}$$

where now

$$F_{reg}^{(3)} = \frac{\mathrm{Tr}(M_2^n)}{\mathrm{Tr}(M_1^n)}. \tag{37}$$

Consequently,

$$P_{active}([A], n) = \alpha \frac{1}{1 + \frac{1}{F_{reg}^{(3)}([A],n)} \frac{K_P}{[P]}}. \tag{38}$$

See Figure 5 for an example of the predictions of Model 3.

Appendix: Traces of M_1 and M_2

The trace of

$$M_1 = \begin{pmatrix} e^{-\beta(K+N)} & e^{-\beta K/2} \\ e^{-\beta K/2} & 1 \end{pmatrix} = \begin{pmatrix} \frac{[A]}{K_A}e^{-\beta N} & \sqrt{\frac{[A]}{K_A}} \\ \sqrt{\frac{[A]}{K_A}} & 1 \end{pmatrix} \qquad (39)$$

is given by

$$
\begin{aligned}
\text{Tr}(M_1^n) &= 2^{-n}\left[\frac{[A]}{K_A}e^{-\beta N} - \sqrt{\frac{[A]}{K_A}\left(e^{-\beta N}\left(\frac{[A]}{K_A}e^{-\beta N} - 2\right) + 4\right) + 1} + 1\right]^n \\
&+ 2^{-n}\left[\frac{[A]}{K_A}e^{-\beta N} + \sqrt{\frac{[A]}{K_A}\left(e^{-\beta N}\left(\frac{[A]}{K_A}e^{-\beta N} - 2\right) + 4\right) + 1} + 1\right]^n.
\end{aligned}
$$

The trace of

$$M_2 = \begin{pmatrix} e^{-\beta(K+L+N)} & e^{-\beta(K+L)/2} \\ e^{-\beta(K+L)/2} & 1 \end{pmatrix} = \begin{pmatrix} \frac{[A]}{K_A}e^{-\beta(L+N)} & \sqrt{\frac{[A]}{K_A}e^{-\beta N}} \\ \sqrt{\frac{[A]}{K_A}e^{-\beta N}} & 1 \end{pmatrix} \qquad (40)$$

is given by

$$
\begin{aligned}
\text{Tr}(M_2^n) &= 2^{-n}\left[\frac{[A]}{K_A}e^{-\beta(L+N)} - \sqrt{\frac{[A]}{K_A}e^{-\beta L}\left(e^{-\beta N}\left(\frac{[A]}{K_A}e^{-\beta(L+N)} - 2\right) + 4\right) + 1} + 1\right]^n \\
&+ 2^{-n}\left[\frac{[A]}{K_A}e^{-\beta(L+N)} + \sqrt{\frac{[A]}{K_A}e^{-\beta L}\left(e^{-\beta N}\left(\frac{[A]}{K_A}e^{-\beta(L+N)} - 2\right) + 4\right) + 1} + 1\right]^n.
\end{aligned}
$$

References

[1] Hoffmann, A., Leung, T.H., and Baltimore, D. (2003). Genetic analysis of NF-kB/Rel transcription factors defines functional specificities. EMBO J **22**, 5530-5539.

[2] Bosisio, D., Marazzi, I., Agresti, A., Shimizu, N., Bianchi, M.E., and Natoli, G. (2006). A hyper-dynamic equilibrium between promoter-bound and nucleoplasmic dimers controls NF-kappaB-dependent gene activity. EMBO J **25**, 798-810.

[3] Darzacq, X., Shav-Tal, Y., de Turris, V., Brody, Y., Shenoy, S.M., Phair, R.D., and Singer, R.H. (2007). In vivo dynamics of RNA polymerase II transcription. Nat Struct Mol Biol **14**, 796-806.

[4] K. Huang, *Statistical Mechanics*, Wiley 1987

[5] Raser M. R. and O'Shea E. K. (2005). Noise in gene expression: Origins, consequences, and control. Science **309**, 2010-2013.

[6] Bintu, L., Buchler, N.E., Garcia, H.G., Gerland, U., Hwa, T., Kondev, J., and Phillips, R. (2005). Transcriptional regulation by the numbers: models. Curr Opin Genet Dev **15**, 116-124.